Fabrication of Surface Metal Matrix Composites Using Friction Stir Processing

by

Saman Sahraeinejad

A thesis
presented to the University of Waterloo
in fulfillment of the
thesis requirement for the degree of
Master of Applied Science
in
Mechanical Engineering

Waterloo, Ontario, Canada, Year

AUTHOR'S DECLARATION

I hereby declare that I am the sole author of this thesis. This is a true copy of the thesis, including any required final revisions, as accepted by my examiners.

I understand that my thesis may be made electronically available to the public.

Abstract

Friction stir processing has been employed to produce metal matrix composites by incorporating reinforcement particles in an Al 5059 matrix. Various particles with sizes from 130 nm to 4.3 μm, and different process parameters, were examined to obtain a uniform distribution of particles within the processed region. Mechanical properties (*i.e.* tensile and microhardness) of the Al 5059 matrix metal matrix composites reinforced with Al_2O_3, SiC, and B_4C were tested and compared. Tensile tests demonstrated increases in yield strength by 20, 32, and 38 percent compared to the matrix alloy for composites containing Al_2O_3, SiC, and B_4C, respectively. The average microhardness value within the stir zone increased from 85 HV in the base material to a maximum of 170 HV in the B_4C-reinforced composite. Particle refinement during friction stir processing was more pronounced with micron-sized particles, and virtually insignificant for nano-sized particles. Nano-scale particles seem to be more efficient in increasing the hardness when a similar fraction is used compared to micro-sized particles.

Acknowledgements

I would like to express the sincere appreciation to my supervisor professor Adrian Gerlich, who has shown the attitude and the substance of a genius: he continually and persuasively conveyed a spirit of adventure in regard to research and scholarship, and an excitement in regard to teaching. Without his supervision and constant help writing of this thesis would not have been possible.

Dedication

I dedicate this thesis to my wife, Minoo, for her love, support, and encouragement each step of the way.

Table of Contents

List of Figures

List of Tables

.

Chapter 1
Introduction

Friction stir processing (FSP) is a solid state material processing technique based on the principles of friction stir welding developed by The Welding Institute (TWI) in 1991[1] [2]. The severe plastic deformation and stirring action imposed by the tool during FSP has created many interesting applications for this process [3]. Examples are microstructural modification and homogenization of cast alloys and powder metallurgy fabricated parts [1, 4-9] and production and homogenization of metal matrix composites [10-16]. In particular, composite fabrication by FSP has recently attracted much interest and a great deal of research work has been done on this subject. Production of defect-free bulk and surface composites has been reported for different MMCs such as aluminum matrix composites (Al/SiC [17-21], Al/Al_2O_3 [22, 23], Al/NiTi [24], Al/CNT [25-27], Al/Fullerene [28], Al/Ni [29], Al/TiO_2 [30]), magnesium matrix composites (AZ31/nano ZrO_2 and nano SiO_2 [31], AZ61/ SiO_2 [16], AZ31/SiC [32], AZ31/CNT [15], AZ31/C_{60} [33]), copper matrix composites (Cu/SiC [34], Cu/CNT [35]) and steel matrix composites (L316/SiC [36], mild steel/nano TiC [37]). Generally the process involves the incorporation of the reinforcement into a groove or holes on the surface of the metal matrix plate and then applying FSP to mix the two. When the stirring tool passes through this material it effectively distributes the reinforcement within the matrix. However, in addition to difficulties with particle distribution, an important issue that arises during use of this method is how to minimize loss of the inserted particles during the process. This is important because uncontrolled loss of reinforcement introduces the problem of control over the amount of reinforcement, since the material loss makes it impossible to achieve a target percentage of secondary material during the fabrication procedure. The most widely used solutionto this issue is to insert the particles into the groove and perform one FSP pass with a cylindrical tool having no pin before starting the actual FSP using the typical FSP tool [16, 22]. In a different approach Lim *et al.* [25] and Mahmoud *et al.* [25, 38] have covered the groove with a thin plate and then applied FSP on this plate along the groove. This method successfully prevents material loss, however making a bond between the original plate and the “cover plate” remains an issue and needs special tool design and careful control of other process parameters. Some other researchers [39-42] have used a more complicated procedure; they have first prepared a powder preform using conventional powder metallurgy and then inserted it into the groove. This method seems to be applicable for in-situ composites [40-42], or in

composites where the reinforcement is not a ceramic particle or nano-sized material [39], since compacting such materials involves special equipment and high pressures.

Tool geometry and FSP process parameters are the key factors that may be altered to achieve uniform distribution of the secondary material. It is shown that varying the process parameters may affect particle distribution in different ways; by applying low axial force or low target depth, it has been found that the particles will not distribute at all whereas with high axial force or high target depth, all the particles will be pushed away from the pin surface. Hence, a moderate depth can provide the best distribution [17, 23]. Increasing travel speed may lead to lower heat input which could result in insufficient martial flow for optimal particle distribution [15], and so repeated FSP passes may be needed to improve distribution by introducing more stirring and mixing [23, 31, 43]. It is generally accepted that increasing the rotation speed and decreasing the travel speed improves particle distribution [15, 44]. This is attributed to the better stirring and mixing as a result of higher heat input. However, Mahmoud *et al.* have reported the best particle distribution was obtained by decreasing the rotation speed to as low as possible to achieve a defect-free nugget, though no detailed explanation of the reasons were provided [38, 43]. On the other hand, one should consider that increasing the heat input results in larger grains in the final matrix microstructure [3] which is detrimental to mechanical properties. Therefore optimum process parameters must be determined for each specific application.

The effect of tool pin profile on particle distribution has been also investigated. Mahmoud *et al.* [38] have shown that SiC particles were distributed more homogeneously in aluminum when a square probe tool was used compared to circular or triangular probe tools [38]. Azizieh *et al.* have studied the effect of threads and flutes on the surface of the pin in fabrication of AZ31/ Al_2O_3 composites by FSP and reported the best particle distribution occurs with a threaded pin without flutes [44]. Vijay and Murugan [45] have friction stir welded Al/TiB_2 composite samples with tools having square, hexagon or octagon pin geometry and concluded that a straight square pin achieves the best mechanical properties [45], which implies a uniform TiB_2 distribution is achieved. A similar approach was used to produce Al 5059/MWCNT composite, as published elsewhere [27]. In particular, Al–B_4C composites offer not only the potential for surface hardening, but also the special capability in nuclear applications to absorb thermal neutrons, thus it is being used as the main neutron shielding material in the nuclear industry [46]. B_4C provides outstanding physical and mechanical properties such as such as high impact and wear resistance, low density, high melting point, high hardness, and good thermal

and electrical conductivity [47]. Therefore, a homogenous distribution of B_4C particles in the matrix is always desirable to achieve consistent neutron absorption properties.

In this study, a refined composite fabrication procedure via FSP is proposed. This new approach is based on details of material flow imposed by different tool geometries and applies the effect of process parameters to achieve uniform distribution of the secondary particles. Multiple FSP passes were applied to promote material mixing, generating a uniform dispersion of particles. Different reinforcing materials were examined to evaluate the applicability of the suggested technique. Therefore, the objective of this work is to study the microstructure and the mechanical behavior of, Al 5059 matrix composites fabricated using the new FSP method and reinforced with various particle types and sizes. The strengthening mechanism in mechanical behavior as determined using uniaxial tensile and hardness tests, and fracture behaviour of the friction stir processed particle reinforced composites are then discussed and compared in detail.

Chapter 2

Literature review

2.1 Composite Materials

A composite is a material consisting of two or more materials that are *synthetically made,* dissimilar to one that develops naturally. A composite material, also, must include chemically different constituent phases which are separated by a clear interface. Although, most metallic alloys and many ceramics have multiple phases, they not fit this definition because they materialize as a result of natural phenomena. Numerous composite materials are comprised of just two phases; one is known as the **matrix,** which continuously surrounds the other constituent, which is called the **dispersed phase.** The properties of the component phases (i.e., volume fraction, shape, and size of particles, distribution, and orientation) define the properties of the composite[48].

Considering the type and the shape of reinforcement used in fabricating the final material, composites can be classified in three main categories as shown in Figure 1, consisting of particle-reinforced, fiber-reinforced, and structural composites. Each group includes a minimum of two subdivisions. Equiaxed dispersed phase is the main characteristic of particle-reinforced composites (i.e., particle dimensions are nearly the same in all directions); whereas, the dispersed phase of fiber-reinforced composites, has the geometry of a fiber (i.e., a large length-to-diameter ratio). Structural composites are mixtures of composites and homogeneous materials[48].

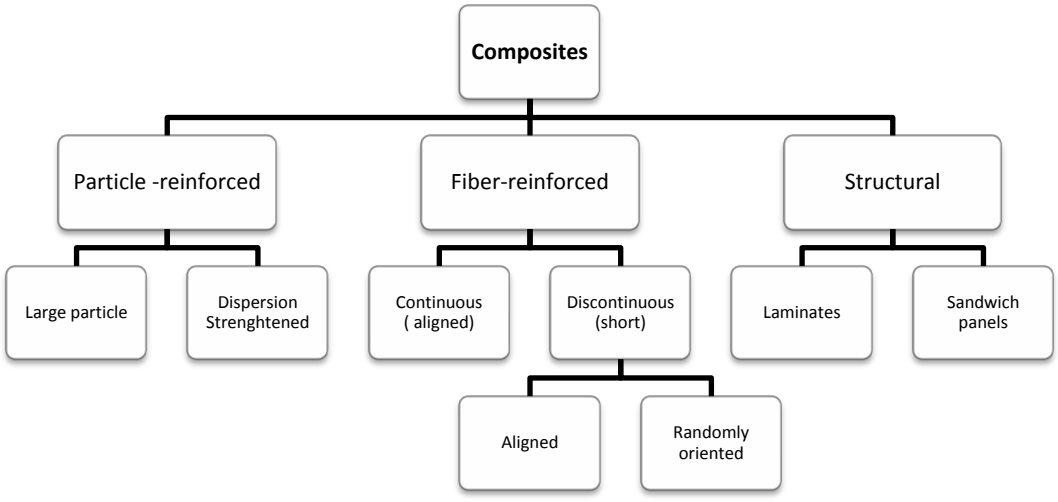

Figure 1 Schematic classification for various composites

2.1.1 Particle reinforced composites

Particle-reinforced composites are consisting of two sub- divisions can be found as either **large-particle** or **dispersion-strengthened composites**. These two categories are distinguished by strengthening mechanism that is used to form the composite. When the particle–matrix relations cannot be discussed on the atomic or molecular level, the term “large-particle” is used. The majority of composites in this category consist of harder particulate phases than matrix material. The strengthening particles detain movement of the matrix phase in the neighborhood of each particle. In fact, a portion of utilized stress is conveyed to the particles by matrix. Robust bonding at the matrix–particle interface plays an important role in improvement of mechanical behavior of composites. An example of large-particle composite is concrete, which is constituted of cement (the matrix), and sand and gravel (the particulates) [48].

All three material types (metals, polymers, and ceramics) can be applied to develop large-particle composites. Cermets for instance are categorized as large particle ceramic–metal composites. The cemented carbide is the most common cermet which is combined of enormously stiff particles of a refractory carbide ceramic such as tungsten carbide (WC) or titanium carbide (TiC), surrounded in a matrix of a metal such as cobalt or nickel. Cutting tools for hardened steels are widely made out of these type of composites[48].

In contrast to large particle composites, dispersion-strengthened composites include particles with diameters between 10 and 100 nm. The strengthening of the material due to inclusion of the particles takes place on the atomic or molecular level as a result of particle–matrix interactions. The mechanism of strengthening is similar to that for precipitation hardening. The small dispersed particles obstruct the movement of dislocations while the matrix tolerates the major portion of an applied load. Thus, restriction of plastic deformation results in improving yield and tensile strengths, as well as hardness. Efficient strengthening occurs when the particles are small and uniformly dispersed throughout the matrix. The effectiveness of dispersion strengthening is not as prominent as with precipitation hardening; however, since the dispersed particles are generally have to be not reactive with the matrix phase in dispersion strengthened materials, the strengthening is maintained at higher temperatures and for longer time periods. For precipitation-hardened alloys, the improvement in strength may diminish upon heat treatment as a result of precipitate growth or dissolution of the precipitate phase in the matrix material.

The overall performance of a composite is affected by the volume fraction of the two phases. Since in general, increasing the particulate content leads to enhancement of mechanical properties. The dependence of the elastic modulus on the volume fraction of the constituent phases for a two-phase composite has been expressed by two mathematical terms. These **rules of mixtures** equations predict that the elastic modulus should fall between an upper bound represented by [49]:

$$E_c(u) = E_m(V_m) + E_p(V_p) \qquad \textbf{Eq. 1}$$

and a lower bound represented by:

$$E_c(l) = \frac{E_m E_p}{E_p(V_m) + E_m(V_p)} \qquad \textbf{Eq. 2}$$

In these expressions, *E* and *V* denote the elastic modulus and volume fraction, respectively, whereas the subscripts *c*, *m*, and *p* represent composite, matrix, and particulate phases.

Figure 2 shows upper- and lower-bound -versus- curves given by Eq.1 and 2 respectively, for a copper–tungsten composite, in which tungsten is the particulate phase. It can be seen from the figure that experimental data points fall between the two curves.

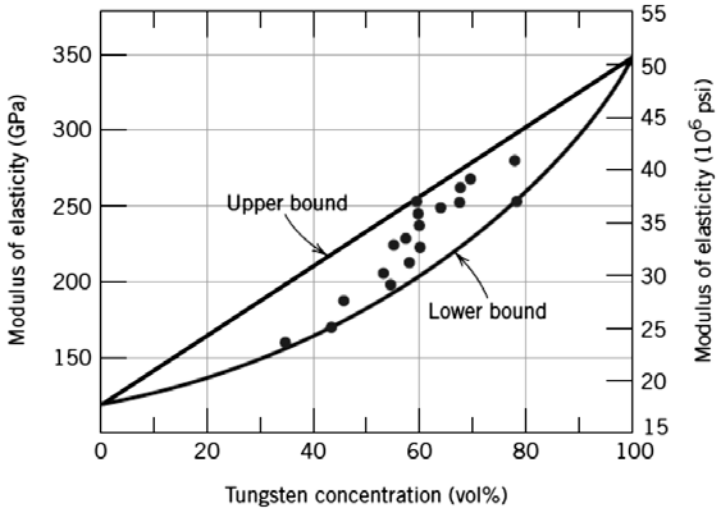

Figure 2: Modulus of elasticity versus volume percent tungsten for a composite of tungsten particles dispersed within a copper matrix. Upper and lower bounds are according to Eq.1 and Eq. 2. [49]

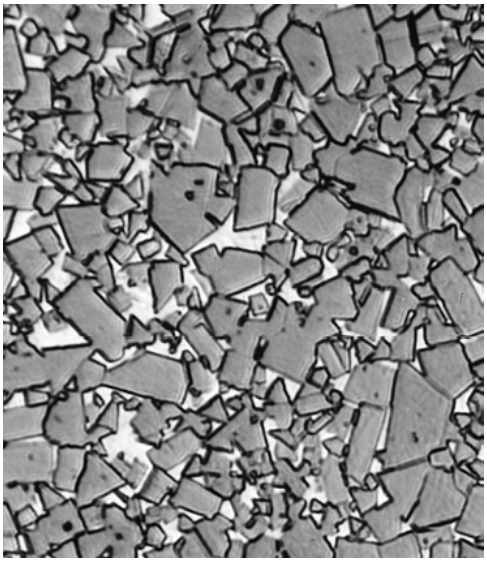

Figure 3: Micrograph of a WC–Co cemented carbide. Light areas are the cobalt matrix; dark regions, the particles of tungsten carbide[48].

2.1.2 Metal Matrix Composites (MMCs)

In a composite, when the matrix is metal, it is termed a Metal-Matrix-Composite, MMC. Many scholars associate the expression 'metal matrix composites' with the term light metal matrix composites [50]. MMCs are usually characterized by the reinforcement: particle-reinforced MMCs, short fiber- or whisker-reinforced MMCs, and continuous fiber- or layered MMCs, as shown schematically in Figure 4 [50].

Aluminum is the dominant choice of matrix material for majority of the metal-matrix composites. However, it must not be considered as the only one[50]; for instance, titanium alloys are employed in MMCs for some specific applications. These titanium alloys have enhanced strength-to-weight ratios as well as improved strength retentions at 400–500 ◦C than those of aluminum alloys. Titanium MMCs are applied in applications where performance is challenged regardless of cost- efficiency[51]. On the other hand, aside from metallic wires, advanced ceramics such as boron, carbon, alumina and silicon carbide are the main materials employed as reinforcements [52]. In general these ceramics are oxides, carbides and nitrides which are employed as reinforcements because of their superior combinations of specific strength and stiffness at both ambient temperature and elevated temperature[51].

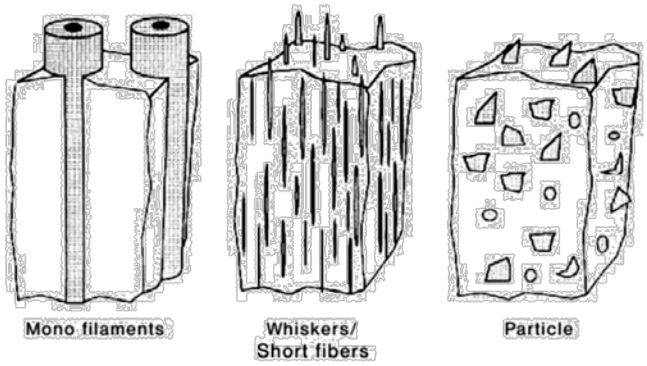

Figure 4: Schematic illustration of three types of metal matrix composite materials[53]

There are several methods to produce metal-matrix composites. Some of these important techniques are explained below.

2.1.2.1 Liquid-State Processes

Casting or liquid infiltration implies infiltration into a fibrous or particulate reinforcement preform by a liquid metal. The poor wetting of ceramic reinforcement by the molten metal during liquid-phase infiltration causes many challenges during MMC fabrication. The reactions between the fiber and the molten metal, which considerably break down the properties of the fiber, are likely to happen when the infiltration of a fiber preform takes place. Applying fiber coatings before infiltration improves wetting and restrains interfacial reactions. In this case, however, the drawback is that the fiber coatings must not be exposed to air prior to infiltration because of the risk of surface oxidation of the coating[54].

Duralcan process is another liquid infiltration process in which ceramic particles and ingot-grade aluminum are mixed and melted to form a MMC (Figure 5). The melted mixture is stirred slightly above the melting temperature (600−700°C). This technique requires particles with sizes ranging between 8−12 μm. In foundry-grade MMCs, high Si aluminum alloys (eg, A356) are implemented, in order to avoid the development of the brittle compound Al4C3, which is formed from the interfacial reaction between Al and SiC. Al4C3 is extremely detrimental to mechanical properties, particularly toughness and corrosion resistance. On the other hand, when the reinforcement is fiber tows of fibers can be passed through a molten metal bath, where the single fibers are wetted by the liquid matrix removed of excess metal, and a composite wire is shaped. A pack of such wires can be consolidated by extrusion to produce a composite.

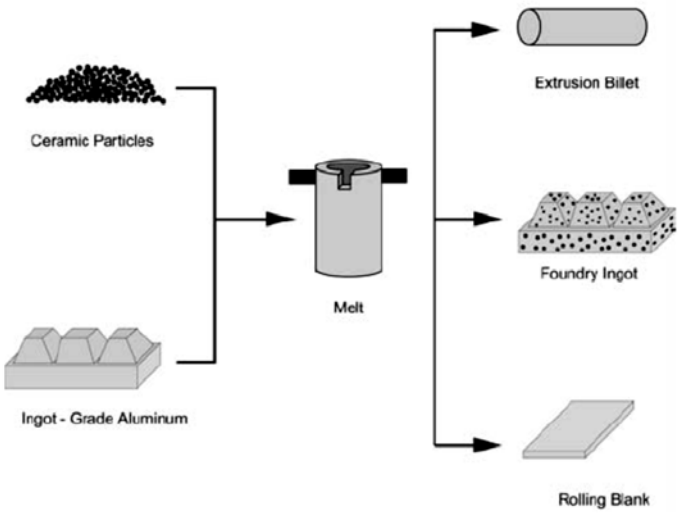

Figure 5: Casting process for particulate or short fiber MMCs

The primex process (Lanxide) is known as another pressure-less liquid metal infiltration process for producing MMCs, which can be utilized with particular reactive metal alloys such as Al− Mg that infiltrate ceramic preforms (Figure 6). For an Al− Mg alloy, in a nitrogen-intense environment, the process occurs between 750−1000°C, and standard infiltration rates are less than 25 cm/h.

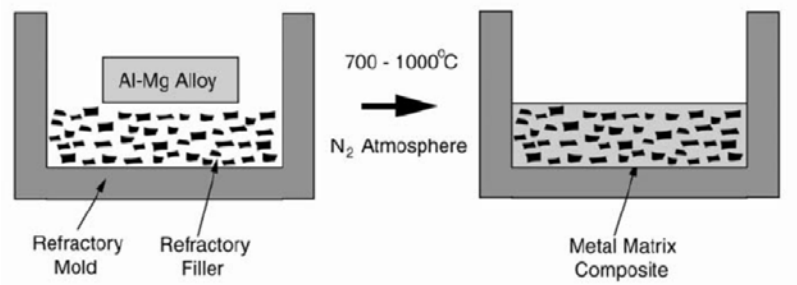

Figure 6: Reactive liquid metal infiltration process [55]

Squeeze casting or pressure infiltration refers to driving a liquid metal into a fibrous or particulate preform [56] (Figure 7). Upon the completion of solidification pressure is applied. As result of this pressure the molten metal passes through miniature aperture in the fibrous preform, so that a good wettability of the reinforcement by the molten metal is not required. The process time in this technique is substantially short. Therefore, the reaction between the reinforcement and molten metal in the produced composite is minimized. Conventional casting defects such as porosity and shrinkage cavities are barely observed in these types of composites[57].

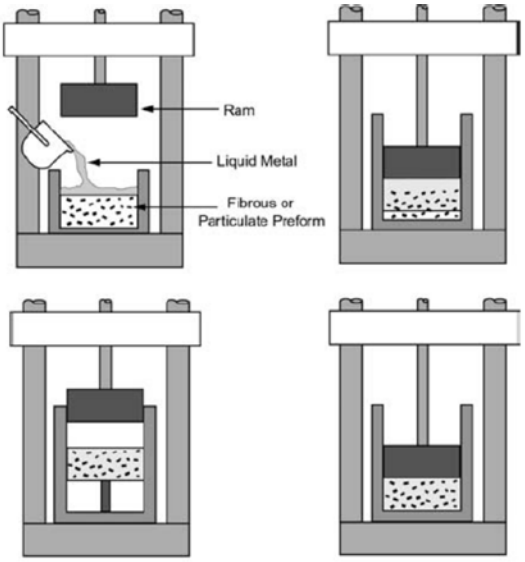

Figure 7: Squeeze casting or pressure infiltration process[57]

2.1.2.2 Solid-State Processes

Diffusion bonding is a conventional solid-state processing method for merging similar or dissimilar metals. The bonds forms as a result of inter-diffusion of atoms between in-contact metallic surfaces at high temperature. As the main advantages, this technique is able to process a broad range of metal matrices and to control fiber orientation and volume fraction. However, long processing times, high processing temperatures and pressures (which leads to a costly process), and a restriction on producing complex profiles are the principle drawbacks of this method. In its present stage of development almost all forms of diffusion bonding processes comprise application of pressure and elevated temperature simultaneously. In this method, matrix alloy foil and fiber arrays (composite wire) or monolayer laminate are pressed in a prearranged order (Figure 8). Vacuum hot pressing is critical phase in the diffusion bonding processes for metal matrix composites. As an alternative of uni-axial pressing, hot iso-static pressing (HIP), may also be applied in which the composite inside the container is consolidated via the gas pressure against a can. The HIP facilitate applying high pressures at high temperatures with inconsistent geometries[50].

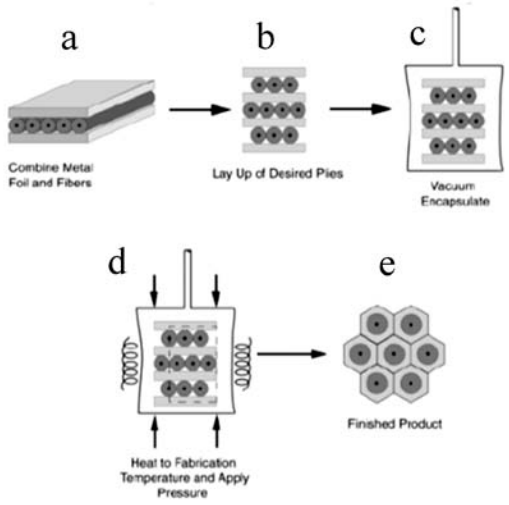

Figure 8: Diffusion bonding process: (a) apply metal foil and cut to shape, (b) layup desired plies, (c) vacuum encapsulate and heat to fabrication temperature, (d) apply pressure and hold for consolidation cycle, and (e) cool, remove, and clean part [50].

Deformation processing is another solid state technique in which the composite material is deformed and/or densified. Mechanical processing (swaging, extrusion, drawing, or rolling) of a ductile two-phases metal−metal composite triggers the two phases to co-deform, leading to one of the phases to elongate and become fibrous in nature within the other phase. The materials produced are occasionally denoted as *in-situ* composites. The characteristics of the preliminary materials define the properties of a deformation processed composite. The initial materials are normally a billet of a two-phase alloy that has been made by casting or powder metallurgy methods[58].

Another conventional practice to produce a laminated composite is roll bonding. The produced composite by this technique consists of distinct metals in layered arrangement which is called sheet laminated metal-matrix composites[59]. The process of producing a laminated MMC using the roll bonding technique is schematically shown in Figure 9.

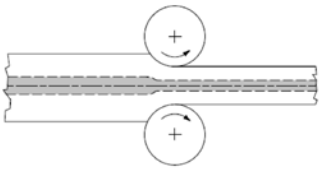

Figure 9: Roll bonding process of making a laminated MMC; a metallurgical bond is produced [59]

Powder processing techniques are utilized to make particulate or short fiber reinforced composites in association with deformation processing. Generally, this method includes cold pressing and sintering or hot pressing to manufacture primarily particle- or whisker-reinforced MMCs[60]. To create a uniform distribution, the matrix and the reinforcement powders are mixed together Figure 10. Cold pressing is applied accordingly to construct a so called green body which is about 80% dense and can be simply processed. To eliminate any absorbed dampness from the particle surfaces the cold pressed green body is preserved in a sealed container and degassed. In order to achieve a completely dense composite, the material is hot pressed either uniaxially or isostatically and extruded. The stiff particles or fibers trigger the matrix to be deformed considerably. Furthermore, dynamic recrystallization at the particle/matrix interface during hot extrusion generates randomly oriented grains near the interface, and moderately textured grains far from the interface.

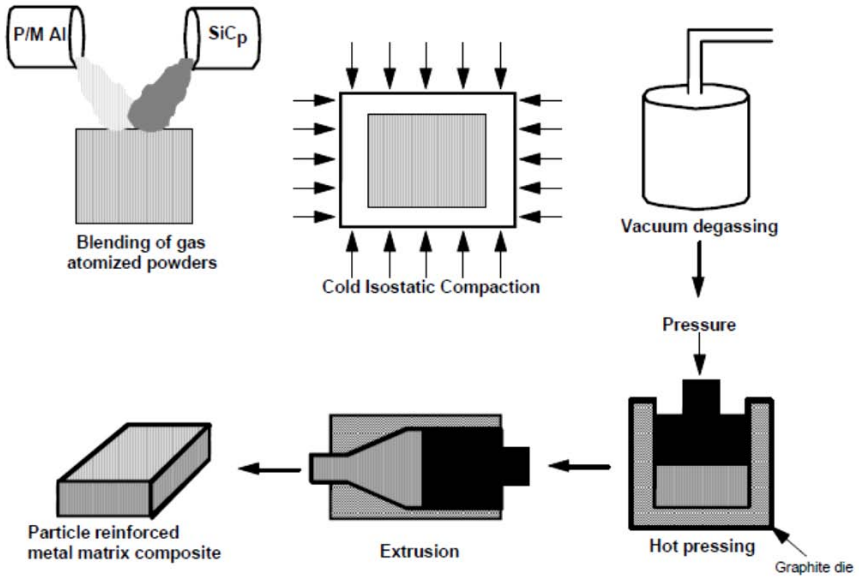

Figure 10 : Powder processing, hot pressing, and extrusion process for fabricating particulate or short fiber reinforced MMCs [60]

Sinter-forging is a unique and economical deformation processing technique [61]. In this method a powder mixture of reinforcement and matrix is cold compacted, sintered, and forged to practically complete solid, see Figure 11. The major benefit of this technique is that forging is carried out to deliver a near-net shape material, leading to minimized the machining operations and material waste. Tensile and fatigue properties of the low cost, sinter-forged composites are equivalent to those of materials produced by extrusion.

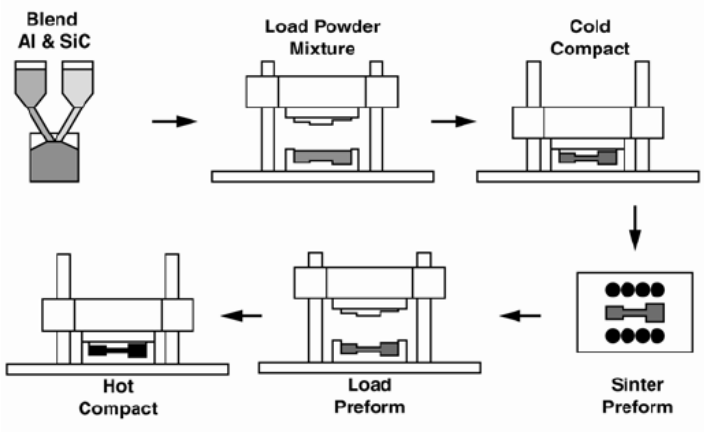

Figure 11: Sinter-forging technique for producing near-net shape, low cost MMCs[61]

2.1.3 Mechanism of reinforcement in MMCs

The characteristics of metal matrix composite materials are determined by their microstructure, constituents, and internal interfaces, which are affected by the processing history. The microstructure covers the structure of the matrix and the reinforced phase. The chemical composition, grain and/or sub-grain size, texture, precipitation behavior and lattice defects are of importance to the matrix. The second phase is characterized by its volume percentage, its composition, size, distribution and orientation. Local varying internal tension effects due to the different thermal expansion behavior of the two phases is an additional influencing factor**.**

The influence of ceramic particles on the strength properties of particle reinforced light metals can be described by using the following micromechanical model[50]:

$$\Delta \boldsymbol{R_{p,c}} = \Delta \boldsymbol{\sigma_{\alpha}} + \Delta \boldsymbol{\sigma_{KG}} + \Delta \boldsymbol{\sigma_{SKG}} + \Delta \boldsymbol{\sigma_{KF}} \qquad \textbf{Eq. 3}$$

where:

$\Delta R_{p,c}$: Increase in tensile strength of aluminum material by particle addition

The influence of induced dislocations is given by:

$$\Delta \boldsymbol{\sigma_{\alpha}} = \boldsymbol{\alpha} \cdot \boldsymbol{G} \cdot \boldsymbol{b} \cdot \boldsymbol{\rho^{1/2}} \qquad \textbf{Eq. 4}$$

with

$$\boldsymbol{\rho} = \boldsymbol{12 \Delta T \frac{\Delta C \phi_P}{bd}} \qquad \textbf{Eq. 5}$$

where

$\Delta\sigma_\alpha$: The yield strength contribution due to geometrical necessary dislocations and inner tension.

α : Constant (values 0.5-1)

G : The shear modulus

b : The burger's vector

ρ : The dislocation density

ΔT : Temperature difference

ΔC : The difference in thermal expansion coefficient between matrix and particle

ϕ_P : The particle volume fraction

d : Particle size

The influence of grain size is given by:

$$\Delta\boldsymbol{\sigma_{KG}} = \boldsymbol{k_{Y1}D^{-1/2}} \qquad \textbf{Eq. 6}$$

with

$$\boldsymbol{D} = \boldsymbol{d}\left(\frac{\boldsymbol{1-\phi_P}}{\boldsymbol{\phi_P}}\right)^{\boldsymbol{1/3}} \qquad \textbf{Eq. 7}$$

where

$\Delta\sigma_{KG}$: The yield strength contribution from changes in grain size (for example recrystallization during thermomechanical treatment of composite materials analogue Hall-Petch)

$$\Delta\boldsymbol{\sigma_{SKG}} = \boldsymbol{k_{Y2}D_s}^{\boldsymbol{-1/2}} \qquad \textbf{Eq. 8}$$

With

$$\boldsymbol{D_s} = \boldsymbol{d}\left(\frac{\boldsymbol{\pi d^2}}{\boldsymbol{6\phi_P}}\right)^{\boldsymbol{1/2}} \qquad \textbf{Eq. 9}$$

where

$\Delta\sigma_{SKG}$: The yield strength contribution due to changes in sub grain size

k_{Y2}: Constant (values 0.05 MN $m^{-3/2}$)

D_s : Resulting sub grain size

ϕ_P : The particle volume fraction

And

$$\Delta\sigma_{KF} = KG\phi_P \left(\frac{2b}{d}\right)^{1/2} . \varepsilon^{1/2} \qquad \textbf{Eq. 10}$$

where

K: Constant

G: shear modulus

ϕ_P : The particle volume fraction

b: The Burger's vector

d: particle diameter

ε: The elongation

The influence of each mechanism on the yield stress is dependent on whether the particle size or the particle content is governs the behavior of the material. Figure 12 shows the example of a particle-strengthened composite material with two different particle diameters. In general, finer particles contribute more to hardening than coarser particles. The influence of grain size and work hardening on the increase in the yield strength are higher than those of other mechanisms when smaller particles are incorporated[50].

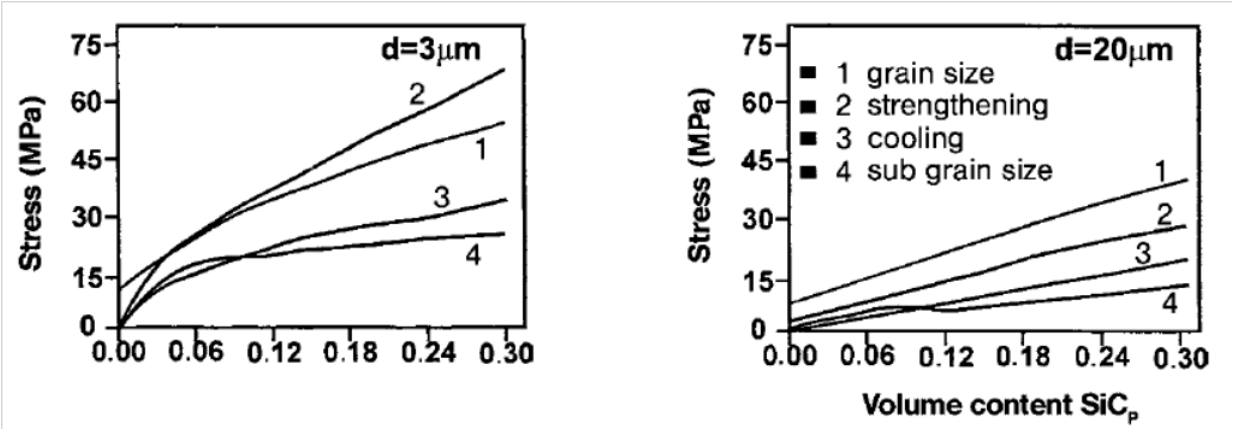

Figure 12 : Strain contribution of different mechanisms to the technical yield point calculated after the micromechanical model for aluminum alloys with SiC_P-addition [62]

2.2 Friction Stir Processing, FSP

Friction stir processing (FSP), is a solid state processing technique that is based on the principles of friction stir welding developed at The Welding Institute (TWI) in 1991. The basic idea of FSP is

rather straightforward. A nonconsumable rotating tool is placed in a single piece of material, and then traversed over the surface of material when the shoulder touches the work piece (Figure 13). The tool heats up the work piece and severely plastically deforms the material. The friction between the tool and work pieces and also the plastic deformation of the material generate heat. The combination of tool rotation and translation caused by localized heating softens the material around the pin and leads to the movement of material from the front to the back of the pin. Initially, FSP was developed by Mishra *et al.,* for microstructural modification [63, 64]. Accordingly, FSP has been employed to produce surface composite on aluminum substrate[65], and the homogenization of powder metallurgy (PM) aluminum alloys, metal matrix composites, and cast aluminum alloys. FSP has definite advantages compared to other metalwork methods. First, FSP is a direct solid-state processing technique that attains microstructural modification, densification, and homogeneity simultaneously. Second, by optimizing the tool design, FSP parameters, and active cooling/heating the microstructure and mechanical properties of the processed zone can be precisely managed. Third, while it is hard to reach an optionally accustomed processed depth using other metalworking procedures; the depth of the processed zone can be optionally controlled by altering the length of the tool pin. Fourth, having a widespread function for the fabrication, processing, and synthesis of materials FSP is an adaptable technique. Fifth, FSP is a green and energy-efficient technique without harmful gas, radiation, and noise since the heat input during FSP comes from friction and plastic deformation. Sixth, FSP does not alter the shape and size of the processed parts[66].

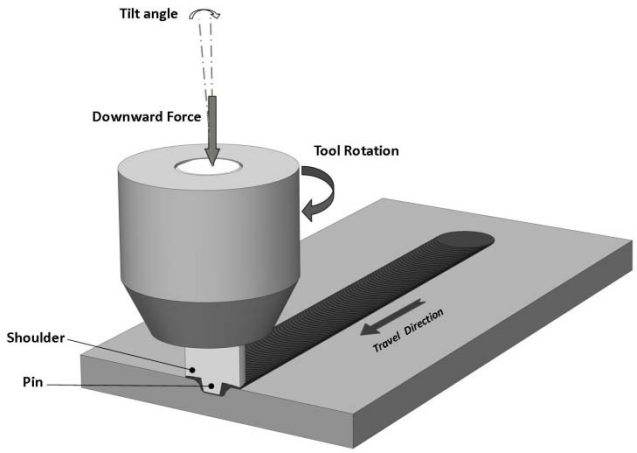

Figure 13: Schematic drawing of FSP

2.2.1 Microstructure evolution during FSP

Due to substantial frictional heating and severe plastic deformation during FSP, dynamic recrystallization occurs in the stirred zone (SZ) resulting in fine and equiaxed recrystallized grains of absolutely uniform size[67]. Thus, the consequential grain microstructure in the SZ is defined by the factors impacting the nucleation and growth of the dynamic recrystallization. Among those factors, the FSP parameters, tool geometry, material chemistry, workpiece temperature, vertical pressure, and active cooling significantly impact on the size of the recrystallized grains in the SZ[67]. Figure 14 shows a characteristic microstructure of FSP 7075Al-T651.

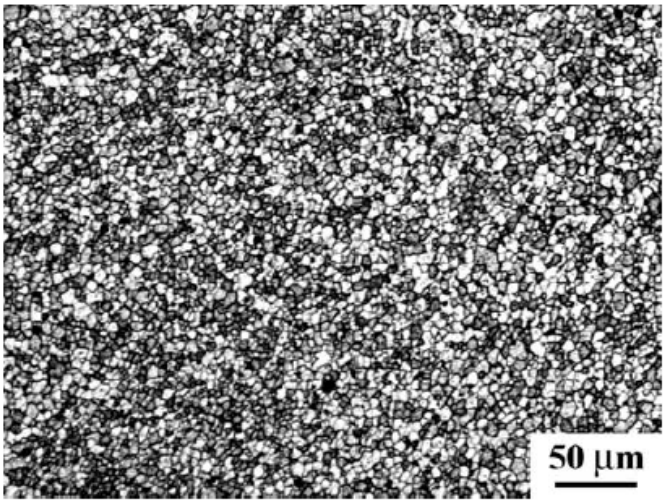

Figure 14: Optical micrograph showing fine and equiaxed gain in FSP 7075Al- T651, at processing parameters of 400 rpm and 102 mm/min[66]

In addition, a high fraction of high-angle boundaries is characteristic of the microstructure in FSP aluminum alloys, as shown in Figure 15. The fraction of high-angle boundaries is as high as 85 to 95 pct[68], which is considerably higher than that achieved in traditional thermo mechanical processed (TMP) aluminum alloys with a typical ratio of 50 to 65 pct [1, 2].

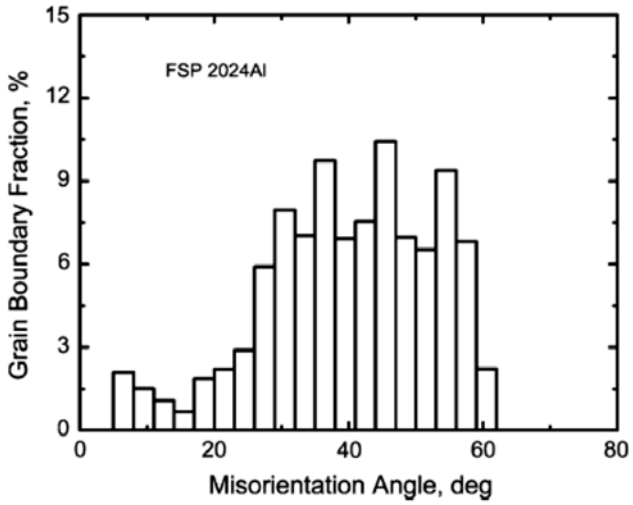

Figure 15: Grain-boundary misorientation distribution in FSP Al 2024 alloy [3]

2.2.2 Mechanical Properties enhancement during FSP

Since altering the FSP parameters, tool design, vertical pressure, and active cooling/heating influence on the grain microstructure, it seems that the mechanical properties of a metallic material can be custom-made through FSP. An increase in both yield strength (YS) and hardness have been reported due to continuously reduction in the grain size of aluminum and magnesium alloys by changing the FSP parameters [4]. The variation trend for YS and hardness fits in the Hall–Petch relationship. A characteristic plot for the Hall–Petch relationship for FSP ZA31 is shown in Figure 16. The grain size reduction leads to an increase in microhardness (HV) of FSP AZ31. In addition, structural superplasticity occurs due to the microstructural refinement in the light alloys by means of FSP. It was reported that the microstructural refinement via FSP resulted in significantly enhanced superplasticity, reduced flow stress, and a shift to higher optimum strain rates and lower temperatures [5].

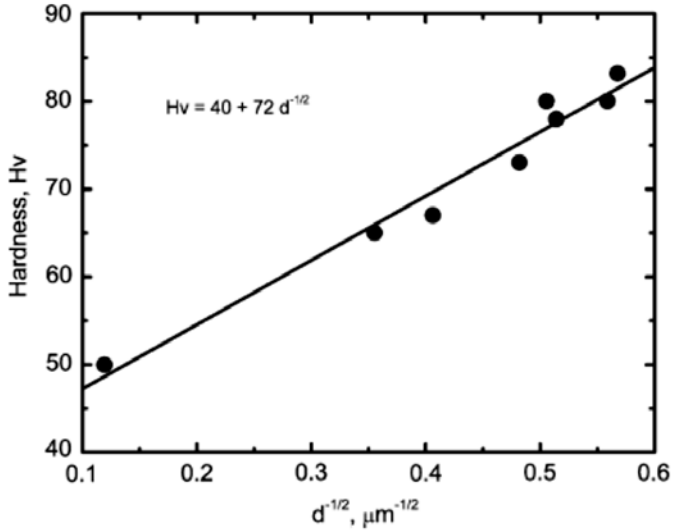

Figure 16: Hall–Petch relationship for FSP AZ31 magnesium alloy [4]

The influence of grain size on the superplasticity of FSP 7075Al alloys as a function of initial strain rate is shown in Figure 17 . The superplastic properties of various FSP alloys, with grain size and optimum strain rate and temperature are reviewed in Table 1. The application of the FSP resulted in the creation of substantial superplasticity in a number of aluminum and magnesium alloys, specially, at high strain rates or low temperatures [5].

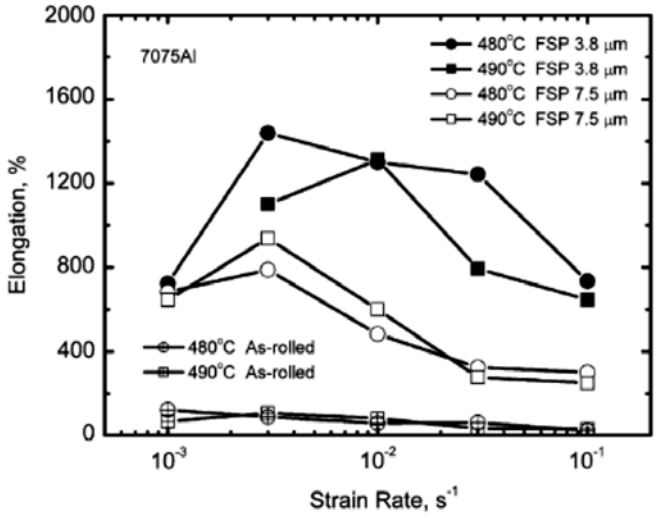

Figure 17: Effect of grain size on superplastic El. of FSP 7075Al-T651,as a function of starin rate [6]

In order to generate the fine-grained materials for superplasticity numerous processing methods such as thermomechanical treatment (TMT), equal channel angular pressing (ECAP), torsion under compression, multi-axial alternative forging (MAF), and accumulative roll bonding (ARB) have been employed. Comparing these technique to the FSP there are certain advantages in FSP which can be noted. First, unlike other processing techniques which are relatively complicated and time-consuming, FSP is a fairly direct processing method that generates a fine-grained microstructure. For instance, TMT comprises solution treatment, over-aging, multiple-pass warm rolling with alternating reheating, and a recrystallization treatment. While at least 4 to 6 passes are required to attain microstructural refinement by ECAP. Second, it is feasible to reach the superplastic forming of thick plates using FSP as it does not decrease the thickness of the processed plates. Whereas, to achieve the fine-grained microstructure to generate the superplastic plates less than 3 mm thick via TMT, a large rolling reduction is required. Third, it is possible to process locally via FSP and create a local grain refinement in a zone that will experience superplastic deformation. While, microstructural refinement on a selective basis is not promising through other processing methods.

Table 1: A summary of superplastic properties of FSP Aluminum and Magnesium Alloys

Materials	Grain Size (μm)	Temperature (°C)	Strain Rate (s^{-1})	Specimen Orientation/Geometry*	El. (Pct)	Reference
7075	3.8	480	1×10^{-2}	T/mini size	1250	19
2024	3.9	430	1×10^{-2}	T/mini size	525	41
5083	6	530	3×10^{-3}	T/mini size	590	46
Al-4Mg-1Zr	1.5	525	1×10^{-1}	T/mini size	1280	47, 48
Al-4Mg-1Zr	0.7	175	1×10^{-4}	T/mini size	240	36
Al-8.9Zn-2.6Mg-0.09Sc	0.7	310	3×10^{-2}	T/mini size	1165	49
A356	~3.0	530	1×10^{-3}	T/mini size	650	50
AZ91	4	300	5×10^{-4}	L/full size	~1200	51
AM60B	4	250	1×10^{-4}	L/full size	~970	52
7075	—	460	1×10^{-3}	L/full size	~800	53
7475	—	460	2×10^{-4}	L/full size	670	54

*T-orientation: The gage length (1.3 mm) of the minitension specimens is at the center of the SZ on the traverse section of the FSP samples. L-orientation: The gage length of full-sized specimens is within the SZ along the FSP direction.

2.2.3 Friction stir processing tool design

As a result of the different geometrical features of the tools the material flow around the tool pin is particularly complex and significantly dissimilar from one tool to the other. Accordingly, the FSP tools can be categorized in three groups as shown in Figure 18. The fixed pin tool is a single piece including the shoulder and pin (Figure 18a). Having an invariable pin length, this type of tool is suitable to process a workpiece with a constant thickness. The adjustable tool includes two pieces, which shoulder and pin move independently, to allow tuning of the pin length during FSP (Figure 18b) [7]. The shoulder and pin, in this design, can be fabricated employing different materials. Also, the worn or broken probe can be simply substituted. Moreover, using an adjustable tool, it is possible to process inconsistent and multiple gauge thickness workpieces. Also, the key hole, left at the end of the friction stir processing seam can be easily filled by using an adjustable tool [8]. The bobbin type tool (Figure 18c) includes three pieces: top shoulder, probe and bottom shoulder [9]. The adjustable pin length between the top and bottom shoulders, in this type of tool, allows it to covers multiple gauge thicknesses. [10].

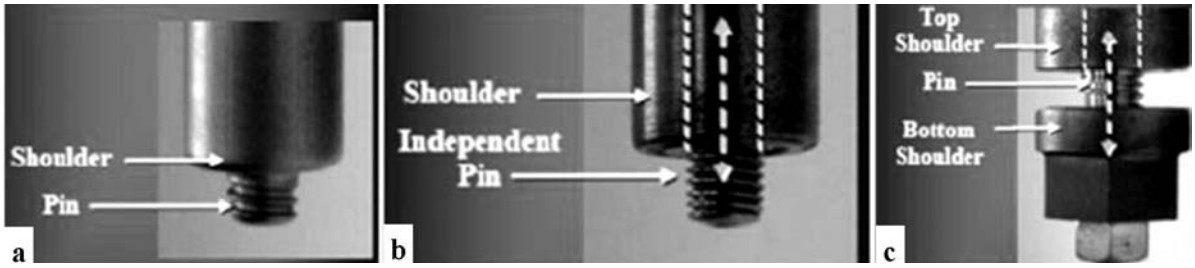

Figure 18: FSP different types of tools. a) fixed, b) adjustable, c) bobbin

2.2.3.1 Tool shapes

Tool shoulder components are basically designed to generate frictional heat and apply the required downward force to consolidate and maintain the soften metal underneath of shoulder surface. The standard shoulder outer surfaces, the bottom end surfaces and the end features are summarized in Figure 19. Generally, the shoulder outer surface includes a cylindrical or conical profile. Since the shoulder plunge depth is usually small (1–5% of the gauge thickness) the influence of the shape of the shoulder outer surface (cylindrical or conical) is believed to be minor [11].

Three varieties of shoulder end surfaces are illustrated in Figure 19. The most straightforward design is the flat shoulder end surface. This type of shoulder is not able to entrap the flowing material under the shoulder surface and causes the formation of unwarranted material flash. A concave shoulder end surface, however, is designed to restrict the material extrusion from the edges of the shoulder [12]. Another viable end shape of the shoulder is a convex profile [13]. When using a convex shoulder profile for joining to workpieces via friction stir welding, the major benefit is that the contact with the workpiece can be achieved at any location down the convex end surface. Thus, variation in flatness or thickness between the two adjoining workpieces can be easily adjusted. On the other hand, the failure to avoid material displacement away from pin leads to an unreliable weld using a convex shoulder profile [8].

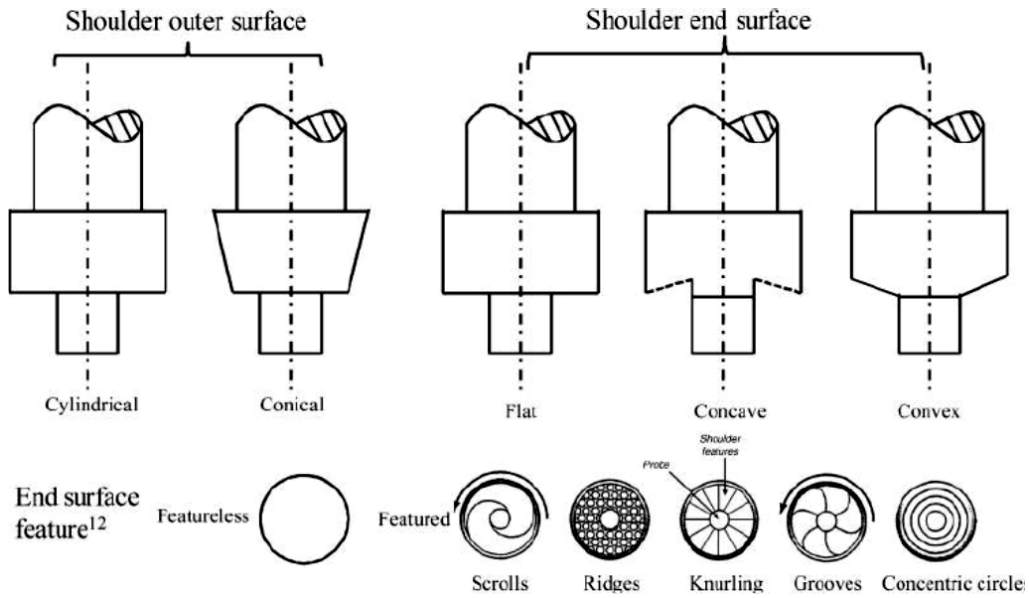

Figure 19: FSP tool shoulder shapes and features [8]

In order to improve mixing quality some features can be added to the shoulder end surfaces to increase material friction, shear and deformation. Normally, shoulder end surfaces contain scrolls, ridges, knurling, grooves and concentric circles [14], as shown in Figure 19. These features can be utilized to concave, flat or convex shoulder ends. The most frequently used shoulder feature is scroll which consists of a flat end surface with a spiral channel cut from the edge towards the centre. The channels facilitate the material flow from the edge of the shoulder to the pin. This way the need to tilt the tool will be avoided [8].

The Tool Pin is mainly responsible for distributing the contacting surface of workpiece, cut the material in front of the tool and drag the material behind the tool. The depth of the deformation and maximum tool travel speed are controlled by the pin geometry. As categorized in Figure 20, the tip of the pin can be either flat or round. Since the convenience of manufacturing a flat tip is greatest, it is the most commonly used geometry. This type of pin induces excessive forging force during the penetration phase. The domed tip shape, however, as result of lower forging force during the plunging, induces less tool wear leading to longer tool life by removing local stress concentration [8].

The FSP tool pin may have either a cylindrical outer surface or a tapered shape. A tapered pin, generally, has larger contact area with the workpiece leading to elevated frictional heat and increasing the plastic deformation. Although, causes severe tool wear, the tapered shape, also, induces a high

hydrostatic pressure in the process zone which is particularly critical for enhancing the material stirring and the nugget uniformity [8].

Various shapes and features can be considered on the pin outer surface including threads, flats or flutes. For processing high strength or extremely abrasive alloys thread-less pins are better choices as the threaded features can be easily worn away. However, the most common type of outer surface feature is the thread. In particular, a left hand threaded pin under clockwise rotation produces a downward material flow by the threads along the probe surface [15]. It is, also, been found that flat features on the pin surface, increasing the local deformation and turbulent flow of the plasticized material, can alter the material movement around the pin [16]. The main function of flats on the pin is analogus to the edge of a cutter. The material is wrapped in the flats and then released at the back of the pin, promoting efficient mixing [8].

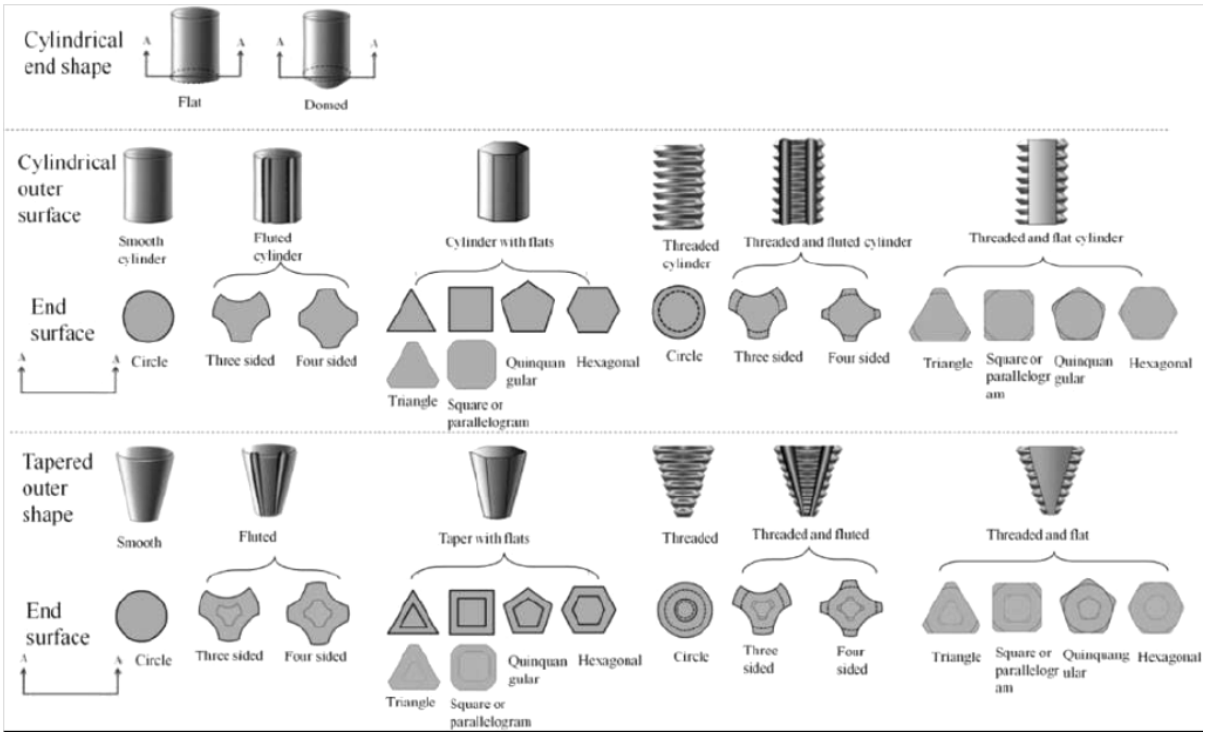

Figure 20: FSP/FSW tool pin shapes [8]

2.2.3.2 Tool dimensions

As demonstrated in Eq. 11, w…hile the heat input depends only linearly on the applied forging force and the rotational speed is a function of the shoulder radius to the third power but [17]. Thus, the energy input in FSP is especially dependent on the shoulder size. Furthermore, the downward forge force is also a function of the shoulder radius.

$$q_0 = 4/3\,\pi^2 \mu P \omega r^3 \qquad \textbf{Eq. 11}$$

Where:

q_0: The net power (W)

μ: Effective friction coefficient

P: Pressure (MPa)

ω: Rotation speed (RPM)

r : Shoulder radius (mm)

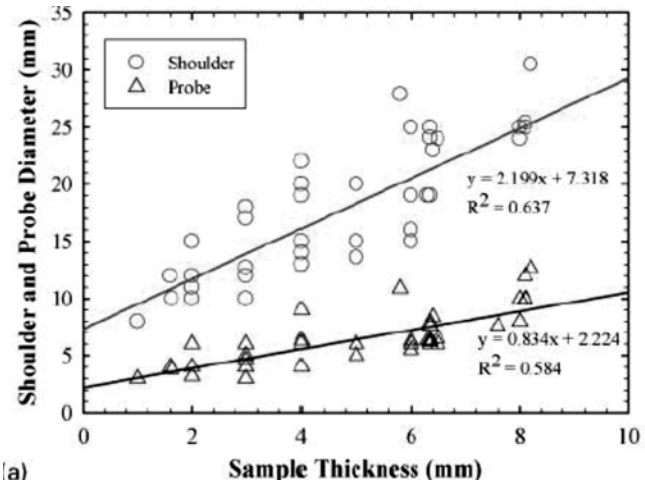

Figure 21: Tool diameters versus workpiece thickness [8]

As shown in Figure 21 a, in which the shoulder diameter as a function of sheet thickness has been reviewed for 53 friction stir welding butt setups, the trend using a least square approximate shows the shoulder diameter is ~2.2 times the sheet thickness plus a constant of 7.3mm [18]. It is well known that with increasing thickness more energy input is needed and therefore a larger shoulder diameter is necessary to generate the heat.

2.2.3.3 Tool materials

The workpiece material and the desired tool life are the two most crucial parameters to indicate the tool material. The following characteristics should be considered when selecting tool material [8]:

a. Superior compressive yield strength at high temperature than the predictable forging force onto tool.
b. Dimensional stability and creep resistance
c. High thermal fatigue strength to endure frequent heating and cooling cycles.
d. Zero destructive reaction with the workpiece material.
e. High fracture toughness to resist the forging force during penetration and dwelling.
f. Minimum coefficient of thermal expansion difference between the pin and the shoulder to reduce the thermal stresses.
g. Good machinability to facilitate cutting complex features on the tool.
h. Reasonable cost.

The most commonly exercised tool material for processing aluminum alloys is tool steel. AISI H13 has been the most frequently used among tool steels. Nickel and cobalt based superalloys, having great strength, ductility, excellent poor creep and corrosion resistance are superior candidate for tool material. The only drawback back which impedes wide application of these superalloys is the difficulty in machining complex features such as flutes and flats on the tool surface. In addition, high temperature strength due to single phase structure of refractory metals, such as tungsten, molybdenum, niobium and tantalum, leads to stable mechanical properties up to 1000-1500°C and making them as good choices for tool material. However, relatively expensive fabrication process of refractory metals (i.e., powder processing). At elevated temperature carbide materials, because of their good wear resistance and sufficient fracture toughness are frequently employed as tool material. Also, ceramic particle reinforced MMCs have been used as tool material although the brittle nature of the composite raises the chance of fracture during the penetration phase. Furthermore, despite the excellent mechanical and thermal properties, extensive application of polycrystalline cubic boron nitride, PCBN, as FSP/FSW tool has been limited due to relatively high manufacturing costs, size limitation and poor machinability [8].

2.2.3.4 Tool wear

Tool wears causes changes to the tool shape leading, potentially causing defects in the stir zone. The tool material and geometry and process parameters define the precise wear mechanism. For instance at low rotation speed the tool wear in PCBN is generally triggered by adhesive wear. Whereas, at high rotation speed the wear is due to abrasive wear [19]. Tool wear has also been reported in processing of Al-20SiC [20] and Al-20Al_2O_3 [21]. AISI oil hardened tool steel with thread on the pin was used. The abrasive particles in the composite caused the thread on the pin get worn away and forming a slightly curve shape pin as shown in Figure 22.

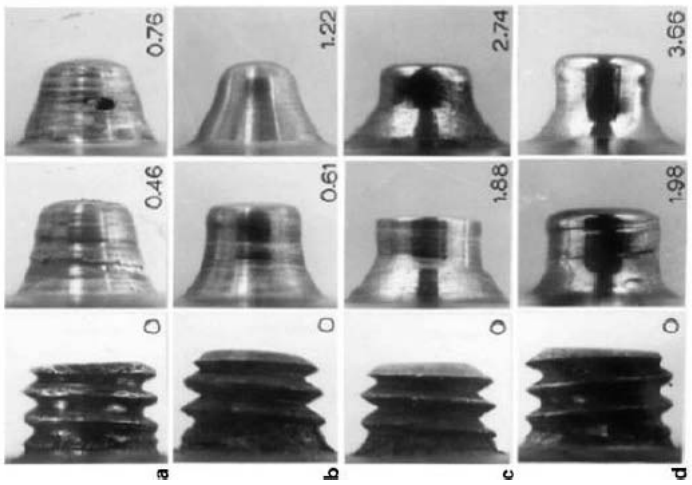

Figure 22: Wear features of probes for Al-MMC at 1000 rpm: welding speeds at a 1, b 3, c 6 and d 9 mm/s [21]

Surprisingly, the worn tool, as was used more, produced more uniform stir zone with no further visible tool wear. This is mainly because of the formation of self-optimized shape on the pin outer surface after intense tool wear. Therefore, utilizing optimized tool shape can significantly minimize the tool consumption even for MMCs. Figure 23 shows the tool wear as a function of weld length for different travel speeds. Thus, perception and designing the material flow around the pin profile in solid state is extremely critical to extend the tool life and improve the process quality.

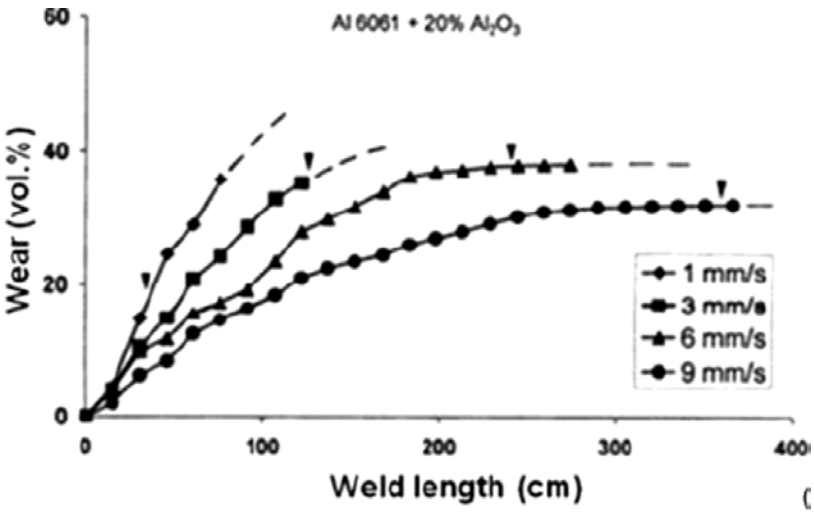

Figure 23: FSP tool pin wear (vol. %) versus weld length [21]

2.3 Fabrication MMCs using FSP

It is well documented that the size and volume fraction of reinforcing phases as well as the characteristics of matrix-reinforcement interface control the mechanical properties of MMCs [22]. Powder metallurgy (P/M) method or molten metal processing have been the main routes to fabricate particle-reinforced metal matrix composites. However, obtaining a uniform dispersion of fine reinforcement particles within the matrix is especially challenging through traditional casting or P/M processing. It is mainly because of the natural trend of fine particles to agglomeration during blending of the matrix and the reinforcement powders.

It has been shown that FSP can be employed to fabricate aluminum matrix composites *in-situ* without supplementary consolidation process. The application of FSP to produce MMCs has the following advantages [23]:

a. Inducing sever plastic deformation to further mixing and refining of constituent phases in the material.

b. Generation of high temperature to ease the *in-situ* reaction to develop reinforcing particles.

c. Causing hot consolidation to establish fully dense solid

On the other hand, the presence of the reinforcement particles in the metallic matrix leads to brittleness which generally is not desirable. Therefore, instead of bulk reinforcement, incorporation of

the particles to the surface enhances the wear properties, which is a surface dependent degradation mode, without sacrificing the bulk properties [24]. However, it is challenging to effectively disperse ceramic particles on a metallic surface by conventional surface treatments. The existing processing techniques to produce surface composites are based on liquid phase processing at elevated temperatures. However, it is tough to prevent interfacial reaction between reinforcement and metal matrix and the development of some harmful phases. In addition, to achieve perfect solidified microstructure in surface layer monitor of processing parameter seems to be crucial. Apparently, processing of surface composite at low temperature, below the melting point, can prevent these problems [25]. In this case, FSP, as a solid state processing technique can be successfully employed to produce surface composites.

Recently FSP has been effectively utilized to fabricate Al-Al_2Cu in-situ composite from Al-Cu powder blend [11], Al–$Al_{13}Fe_4$ in-situ nanocomposite from Al–Fe powder mixtures [26], and Al–Al_3Ti nanocomposite from Al–Ti powder blends [27]. Bulk SiC-reinforced aluminum MMCs, also, has successfully been fabricated by FSP [28]. In another study, multiwalled carbon nanotube, (CNT) was incorporated into aluminum matrix through FSP [29]. Numerous studies have been conducted to investigate fabrication of MMCs by FSP technique. Table 2 summarizes recent nanocomposite fabrication using FSP.

The main difficulty in fabrication of particulate composites is the agglomeration of fine reinforcement particles. By correctly designing the tool shoulder, which mainly generates required frictional and shear force, the tendency of particle agglomeration can be notably moderated. Moreover, the oxide film surrounding reinforcement particles can be broken as a result of large plastic strain in FSP, leading to profound contact between the matrix and the reinforcement and endorses reaction. Multipass FSP combined with pretreatment of reinforcements, also lead to homogenous distribution of super fine particles in the SZ. As the amount of heat input plays the key role in producing a defect free composite optimizing process parameters to generate suitable amount of heat is critical to obtain a sound composite [30].

Table 2 : Summary of the investigations on nanocomposite fabrication using FSP

Study	Materials	Process Parameters		Characteristic studied	Results
		Rotation Speed (rpm)	Travel Speed (mm/min)		
[31]	Magnesium alloy AZ31 and MWCNTs	1500	25	Effect of processing parameters on microstructure, grain refinement and microhardness	• MWCNTs in the composite promoted grain refinement by the FSP. • Good dispersion of the MWCNTs was obtained for the sample FSPed at 25 mm/min and 1,500 rpm. • The FSP with MWCNTs increased the microhardness of the substrates
[32]	Magnesium alloy AZ61and SiO_2 nanoparticles	800	45	Microstructural observations of the nanocomposite formed and mechanical properties	• The yield stress of the FSP composites was improved to 214 MPa in the 1D (one groove) and to 225 MPa in the 2D (two groove) specimens, compared with 140 MPa of the as-received AZ61 billet and 147 MPa of the FSPed AZ61 alloy without silica reinforcement
[33]	Aluminum ally A356 and Al2O3 powder			Vickers microhardness	• The average microhardness values for A356–μAl2O3 and A356–nAl2O3 surface composites were about 90 and 110 HV, respectively
[34]	• Aluminum alloy 6082 and Al2O3 powder	• 1000	• 135	• Grain refinement by multipass FSP, microhardness, and wear behavior of surface composite formed	• The surface composite layer produced by three FSP passes showed a better dispersion of Al2O3 particles. • Almost a three-time increment of the hardness of the parent Al alloy was achieved. • It was observed that wear resistance against a steel disk was significantly improved (two to three times) in the Al/Al2O3 surface nanocomposite layer produced by four FSP passes compared with the as-received Al.

Table 2 (continued)

[35]	Aluminum alloy 6061and nano-Al2O3 particle	480	203.2	Effect of axial force and multipass, hardness values in the composite zone formed	• Larger axial force makes the expanded AMCZ and bonding of AMCZ increases with number of passes. • Pores became smaller and more distributed • FSZ had higher hardness values than other zones due to refined grain size via dynamic recrystallization
[36]	Aluminum alloy 5052- H32, Al2O3 powder	1600	16	Grain size refinement andelongation	• Multiple-pass FSP with the nanosized Al2O3 particles more effectively reduced the grain size of the 5052Al matrix, which ranged from 5.5 to 0.94 μm. • It was observed that an increase in the FSP pass from one to three caused improvement of elongation, especially for stir zone produced without powder. However, elongation decreased in both samples produced by four passes.
[37]	Magnesium alloy AZ91, SiC and Al2O3 powders	900	63	Microhardness of the composite formed	• It was found that with an increase in FSP passes, the average grain size of the SZ decreased. • The average hardness of as-cast AZ91 alloy was found to be 63 HV, which increased to a range from 90 to115 HV with SiC addition and about 105 HV with Al2O3 addition after two passes.

Chapter 3
Experimental Approaches

The as-received matrix material was 6.3 mm thick Al 5059 alloy in the rolled and H131 tempered condition. Al 5059 is a non-heat treatable aluminum alloy and therefore consequent softening in the heat affected zone is not expected after FSP. The nominal composition of Al 5059 is shown in Table 3.

Table 3: Nominal composition of Al 5059

Element	Mg	Mn	Zn	Fe	Si	Ti	Zr
Wt.%	5.26	0.79	0.5	0.09	0.07	0.02	0.12

The rolling resulted in elongated and pancake-shaped microstructure in Al 5059. Elongated precipitates along grain boundaries, which are common in aluminum alloys with high magnesium content, can enhance micro voids formation and coalesce and lead to reduced ductility. Figure 24, illustrates the changes in microstructure in Al5059 as a result of rolling.

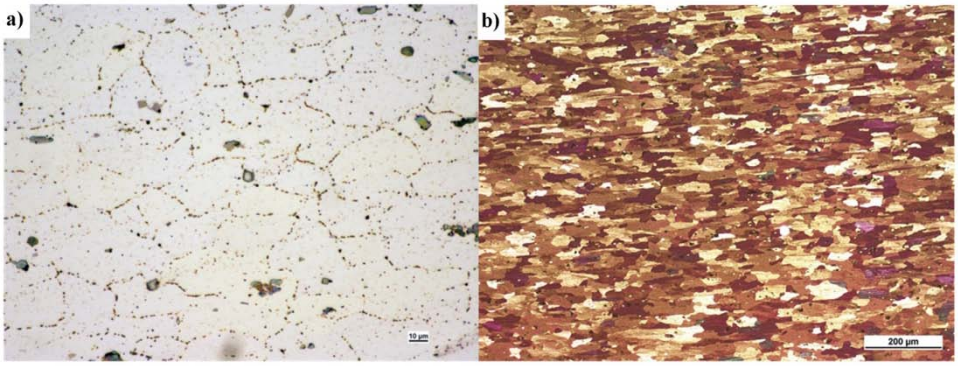

Figure 24: Al5059 microstructure a) before rolling, b) after rolling

For the initial tests to optimize the particle distribution 130 nm Al_2O_3 particles were used as the reinforcement and the final fabrication procedure was also applied successfully to 4.3 µm and 1.1 µm Al_2O_3, 250 nm SiC, and 35 nm B_4C. The average particle size was confirmed by a combination of acoustic particle sizing and electron microscopy observation.

Figure 25: FSP/FSW Machine

A displacement controlled milling machine was used to fabricate the MMC materials (Figure 25). The FSP tools were made from H13 die steel, and heat treated to 46-48 HRC. After heat treatment, tools were coated with a ZrN/TiN multilayer coating to suppress any possible tool wear. Two different tools (cylindrical spiral and 3-flat threaded, as shown in Figure 27) were used in order to disperse the reinforcing particles in the stir zone. It has been suggested that the 3-flat pin geometry provided a matrix microstructure with enhanced strength and ductility compared to the as-received material, and so this was initially investigated for FSP fabrication of the composites [69].

A clamping system was designed in order to maintain the workpiece in position during the process. Two steel blocks clamp the workpiece on top so that the large contact area creates enough force to avoid any movement. The additional set screws ensure that the blocks are positioned horizontally all the time.

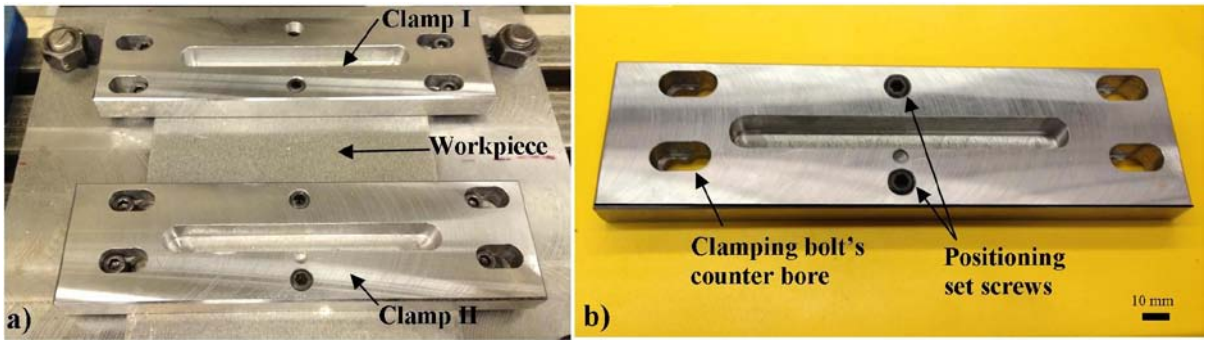

Figure 26: a) FSP clamping system b) specimen clamp

`

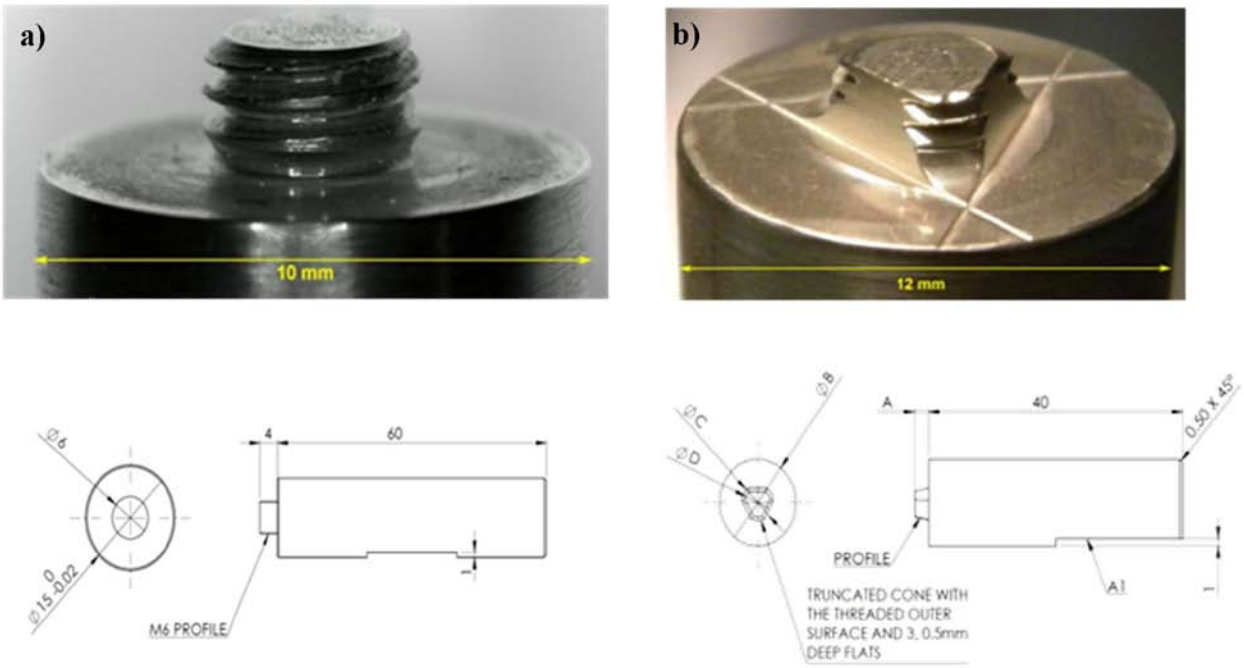

Figure 27: a) conventional threaded-pin tool, b) 3-flat pin tool.

In the present study, the fabrication of composite through FSP is first performed by mixing the reinforcement particles (powders) in the aluminum matrix by machining a groove of 4 mm width and 2 and 4-mm depth in the substrate to accommodate the reinforcement. A cylindrical pin-less tool was then utilized to encapsulate the material in the plate and close the top of the groove via surface deformation (capping pass). Although, the capping pass prevents ejection of the particles from the groove during the FSP, softened thin aluminum layer created at capping pass partially fills the groove

and pushes the particles toward the end of the groove. Therefore, even using the capping pass the volume fraction of the particles will not be the same as the initial powder content.

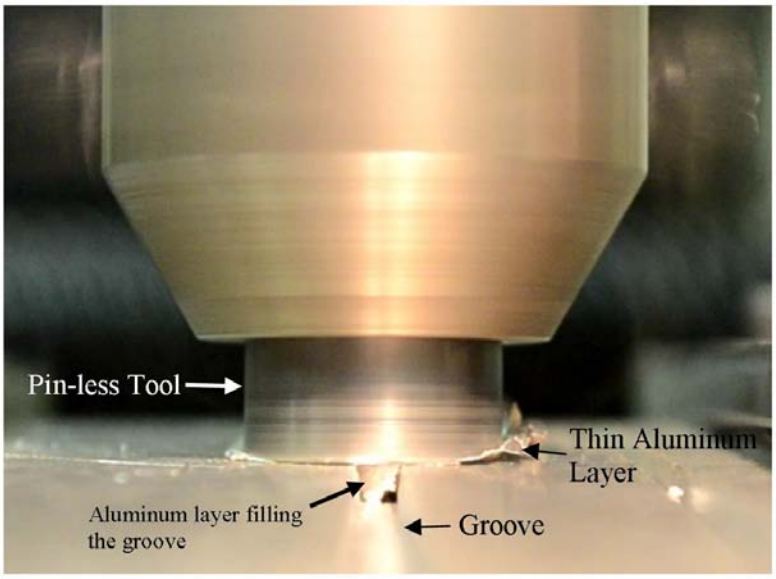

Figure 28: Aluminum film filling the groove during the Capping pass

Upon completion of the capping pass, three passes were performed using different tools described in Table 4.

Table 4: Processing parameters used in the FSP operations with 3-pass technique; travel speeds were 30 mm/min

Pass Number		**Groove Depth (mm)**	**Shoulder Diameter D_1 (mm)**	**Pin Diameter D_2 (mm)**	**Pin Length L_1 (mm)**
0	Capping	N/A	15	N/A	N/A
1	Spiral Pin	2 and 4	10, 15	5	2.2, 4.0
2	3-flat		12, 15	5	2.2, 4.0
3	3-flat		12, 15	5	2.0, 3.8

In order to create an inward material flow within the stir zone during FSP the first and second passes were performed counter clock wise. Therefore, the right hand thread on the pin, while is

rotating CCW, pushes the particles toward the bottom of the stir zone. The third pass, however, was carried out with clock-wise tool rotation to promote movement of the material from bottom of the stir zone toward the surface, resulting in improved vertical uniformity. Process parameters are summarized in Table 5.

Table 5: Summary of FSP Parameters applied

Pass Number		Tool	RPM	Rotation Direction	Inclination (◦)	Travel Speed (mm/min)
0	Capping	Capping	1800	CW		
1	Pass 1	Spiral pin	1120	CCW	2.5	30
2	Pass 2	3 flat	450	CCW	2.5	
3	Pass 3	3 flat	450	CW	2.5	

In order to study the mechanical properties of the composites, uniaxial tensile testing was performed at a constant strain rate of 10^{-3} sec^{-1} by using a Tinius Olsen (H10KT) tensile testing machine. To achieve maximum uniformity, the tensile coupons were machined such that the gauge length of 12.5 mm consisted of only the uniformly distributed regions in the composite material extracted from the stir zone with dimensions of *t* and *w* between 1 to 4 mm (see Figure 29). An extensometer was used to measure the engineering strain. In tensile tests, consistent and repetitive results were obtained with standard deviations between samples processed in comparable fashion were less than 5% (minimum 3 samples per condition).

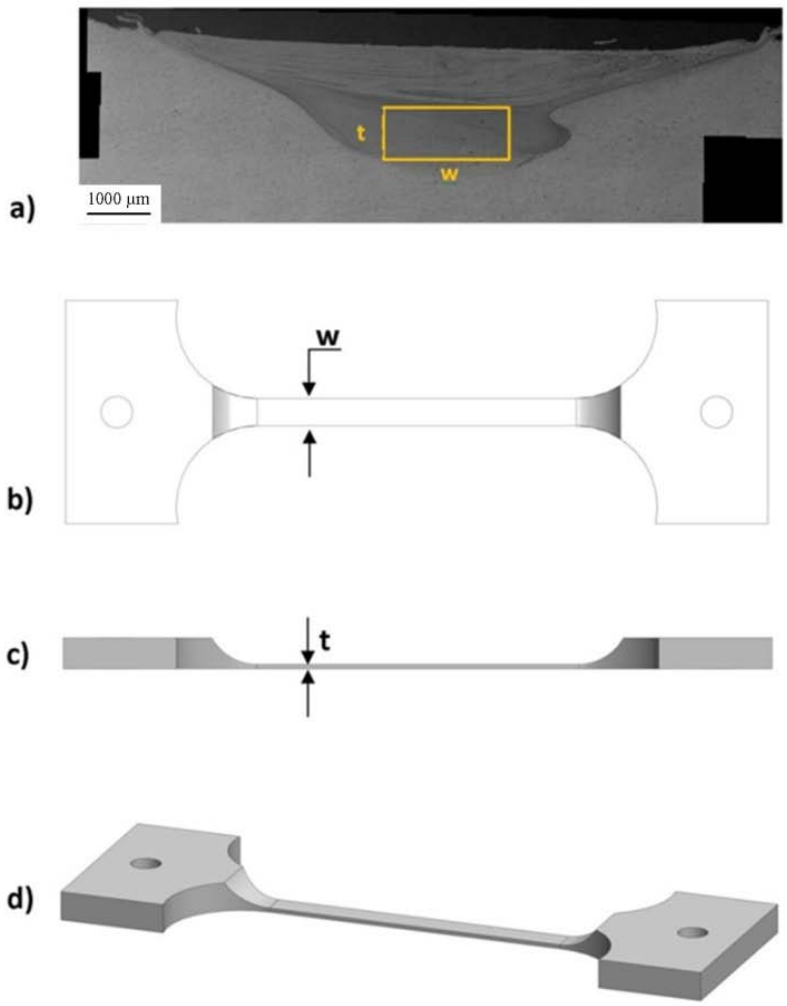

Figure 29: Location and dimensions of the tensile testing coupons.

The fracture surfaces were also examined using SEM. Microhardness indentation measurement was performed on the samples cross sections by a HMV-2000 indenter applying 200 grams load for 15 seconds. Finally, the average of three hardness measurements were reported as measured Vickers hardness number (VHN).

Volume fractions of different particles were measured through energy-dispersive-X-ray spectroscopy, EDX, of each composites. To indicate the fraction of Al_2O_3 and SiC the oxygen and

silicon contents of composites were examined respectively. Having the Silicon and Oxygen content in the composites and using balance equations of SiC and Al_2O_3 the volume fraction can be easily calculated. The EDX analyses were performed in the vicinity of the hardness indentations in order to make a reasonable correlation between a reinforcement volume fraction and the associated hardness. Figure 30 demonstrates an example of EDX analysis for calculating particle volume fraction within the composite. Two spectrums shown in Figure 30 contain different oxygen contents. The average of the two oxygen contents was used to calculate the Al_2O_3 volume fraction in the composite associated with the local microhardness. The same procedure was employed to correlate each microhardness measurement with the volume fraction of reinforced particle at that location. Eq. 12 and 13 were used to calculate the volume fraction of particles based on the constituent contents.

$$4Al + 2O \rightarrow 2Al_2O_3 \qquad \textbf{Eq. 12}$$

$$SiO_2 + 3C \rightarrow 1SiC + 2Co \qquad \textbf{Eq. 13}$$

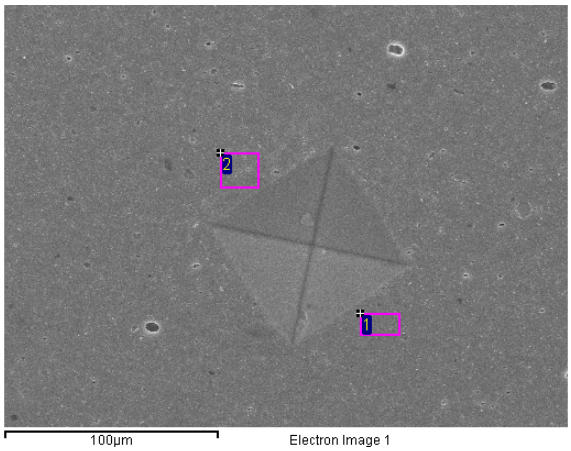

Spectrum	In stats.	O	Mg	Al	Total
Spectrum 1	Yes	3.99	4.88	91.13	100.00
Spectrum 2	Yes	4.66	5.06	90.28	100.00
Max.		4.66	5.06	91.13	
Min.		3.99	4.88	90.28	

Figure 30: EDX analysis at the vicinity of a hardness indentation showing the oxygen content to calculate Al_2O_3 %wt. in Al5059- Al_2O_3 130 nm composite

Chapter 4
Results and Discussion

4.1 Particle distribution

During fabrication of MMCs via FSP, the key issue is establishing a uniform distribution of a reasonably large fraction of reinforcing particles with a given set of processing conditions. Tool geometry and process parameters control the material flow and consolidation of material in the stir zone. One of the main challenges is to achieve a uniform distribution with a single pass, however due to the material flow and intermixing mechanisms which are imposed by the tool, in this research it was not possible to achieve a uniform distribution with a single pass [25]. Figure 31a shows the optical images of a single pass friction stir processed sample with the 3-flat tool. As can be seen, the majority of material is displaced towards the advancing side of the stir zone. Here the zone of plastic flow is insufficient for generating the recirculating flow of material and particles [69]. This has been previously confirmed for different composites produced by one FSP pass [23, 25, 43]. However, when the direction of tool rotation was reversed during the second pass, the particle distribution became more uniform, see Figure 31b.

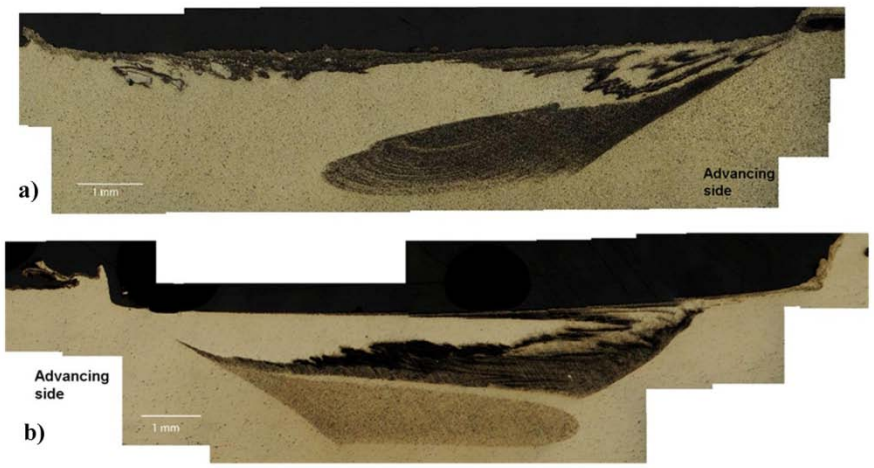

Figure 31: Optical micrographs of cross-sectioned FSP specimens produced using 454 RPM, a travel speed of 20 mm/min, and 4.3 µm alumina particles when (a) one pass is used and (b) two passes are used with a 3-flat tool geometry.

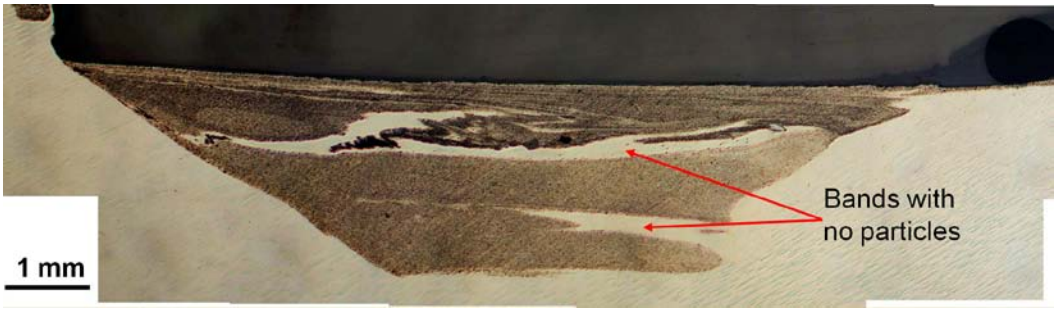

Figure 32: Optical micrograph of cross-sectioned FSP specimen produced using 4.3 µm alumina particles when a 2-pass approach was used with a constant pin length.

The accumulation of particles induced on the advancing side has been balanced by changing the tool rotation direction with alternating passes. However, the distribution in the upper and low regions of the stir zone was quite different, and the hardness distribution was very non-uniform, see Figure 33.

Nevertheless, the particle dispersion remained non-uniform after two passes. As shown in Figure 31b &Figure 32, particles tend to form macro bands, with the areas between those bands free of particles. These macro bands indicate that the stirring after two FSP passes is still insufficient to achieve uniform particle dispersion. The inhomogeneous particle distributions after one and two FSP passes have also been reported in prior work [15, 70, 71]. In order to further improve the distribution of particles from the upper and lower portions of the stir zone, a simple threaded tool (shown in Figure 27a) was used to disperse the particles vertically, before two additional passes were performed using the 3-flat tool which provides a finer matrix grain structure [72]. A threaded pin provides sufficient heat input to ensure material flow by which the reinforced particles can easily move around the tool. Here the tool shoulder and pin (probe) contribute mainly to heat generation and material motion (flow), respectively, causing the softened material to move from the advancing side to the retreating side [73]. Mahmoud et al. [19] showed that particle distribution with an unthreaded probe tend to be concentrated in the bottom areas of the nugget zone. They also observed that particles mainly concentrate on the retreating side of the nugget zone when the threaded probe is employed.

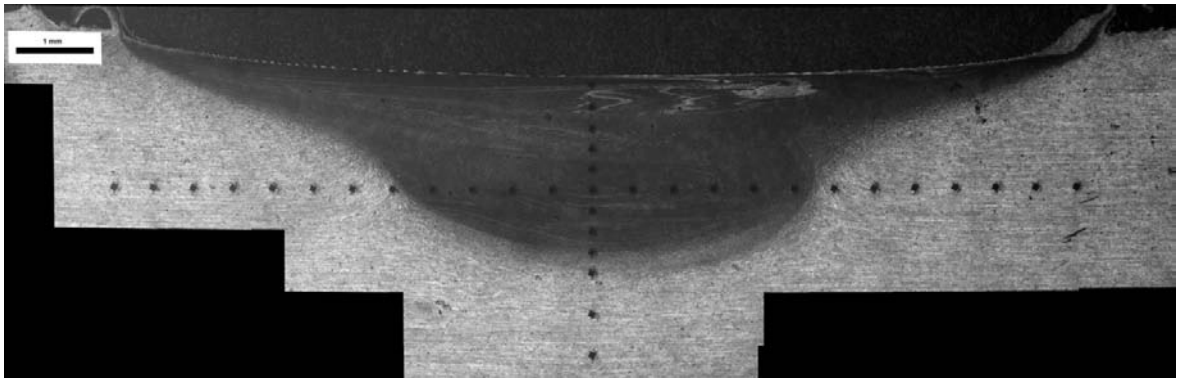

Figure 33: Optical micrograph of cross-sectioned FSP specimen produced using 130 nm alumina particles when a 3-pass approach was used with the parameters described in Table 1 using a 2.2 mm pin and 10 mm shoulder tool for the first and second passes and a 2 mm 3-flat pin for the third pass

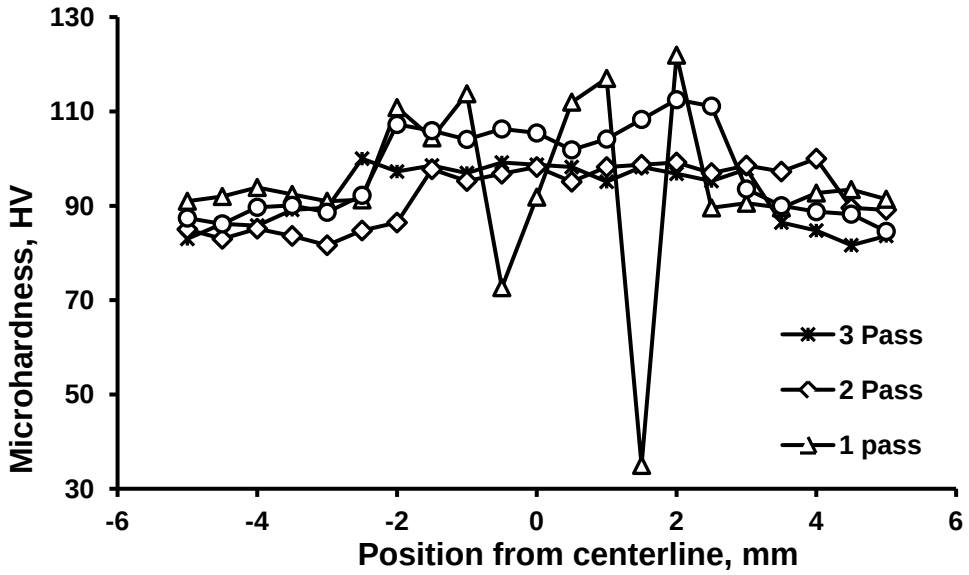

Figure 34: Microhardness profile along stir zone when FSP procedure is conducted in 1 to 3 passes with the parameters indicated in Table 1, and a 1.2 mm deep groove, as well as when 3 passes are used with a 2.0 mm groove.

When the three-pass process was applied, the distribution of reinforcing particles was much more uniform in the upper and lower portions of the stir zone, as shown in Figure 33. This is in agreement with Mahmoud *et al.* [19] findings on the fabrication of SiC particle reinforced aluminum matrix composites through FSP. These are expected to result from the incorporation of the aluminum alloy material on the outer boundary of the stir zone due to the recirculating flow produced by the tool during the final pass. This recirculating flow has been studied in a number of prior studies (for example see [74]).The incorporation of the aluminum alloy material arises from penetration of the tool into the unreinforced matrix material during the final pass. This penetration of the tool occurs as a result of the thermal softening of the material during FSP, and is inevitable since sufficient axial force must be applied in order to prevent formation of voids and defects within the stir zone and achieve uniform particle distribution. In order to avoid incorporating unreinforced aluminum alloy material into the stir zone during the final pass, a 3-flat tool with a slightly shorter pin (2.0 mm rather than 2.2 mm) was used for the third pass. This ensured that when the tool penetrates into the plate, the pin will not mix new material from below the FSP zone into the stir zone. This method allowed a stir zone with a uniform distribution of particles to be produced, with both micro-scale and nano-scale reinforcing particles. Figure 33 shows an optical micrograph of the composite fabricated with the conditions shown in Table 4 and 5 where alumina nanoparticles were used as the reinforcement and the final pass conducted with the slightly shorter pin. As can be seen a uniform distribution of particles is achieved in the stir zone. Based on these results, it is apparent that the dispersion condition could be controlled by the number of passes and the geometry/position of the tool.

4.2 Mechanical testing and fractography

Figure 34 shows Vickers hardness versus position when using different FSP passes. It can be noted that following the first pass, the fluctuation in the hardness is very significant which is due to non-uniform/incomplete mixing of materials and presence of voids in the stir zone. However, with increasing number of passes, the hardness distribution becomes more uniform, where the average hardness increases from 84±3 HV in the base metal to 100±2 HV in the stir zone. This strengthening can be attributed to grain refinement and uniform distribution of the particles imposed by FSP. However we have shown elsewhere that the contribution of grain refinement is not significant, so secondary particle strengthening is likely to be the main factor here. Although distribution of particles in the 3-pass FSP is more homogenous, this does not necessarily raise the hardness as compared with 2-pass FSP presumably due to the agglomeration of particles. Figure 34 also shows hardness values

of a 3-pass friction stir processed composite using a 2-mm groove. An increase of ~15% in the average hardness values is achieved due to the higher particle concentration compared to when a 1.2 mm groove is used

The increased microhardness value in the friction stir processed Al alloy is mainly due to grain refinement induced by dynamic recrystallization during FSP, and Orowan strengthening due to addition of homogenously dispersed particles [12]. The grain size of the matrix is drastically decreased by the FSP with the particles' dispersion. It is likely that grain refinement is promoted by restricted grain growth due to the pinning effect of the particles on the grain boundaries as well as dynamic recrystallization phenomenon [28, 75]. Generally, FSP generates relatively high temperatures which lead to grain growth after dynamic recrystallization [76].

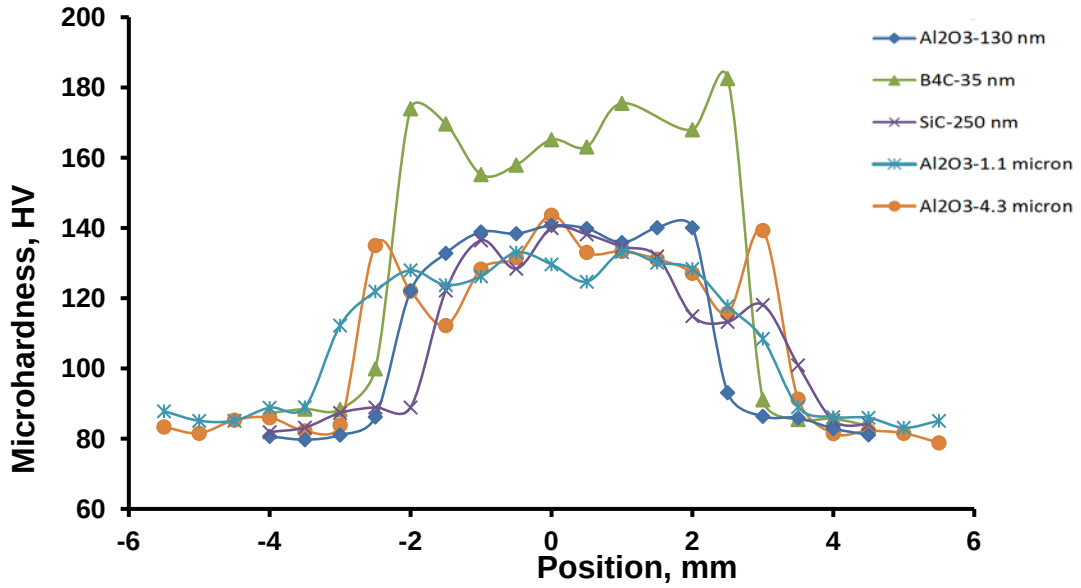

Figure 35: Microhardness profile along stir zone when FSP is conducted using different particles.

Figure 35 shows the hardness distribution when different types of particles (*i.e.* Al_2O_3, SiC and B_4C) with different sizes are employed using identical process parameters. It is clear that the B_4C-reinforced composite exhibits higher hardness values compared to Al_2O_3 and SiC-reinforced composites. This is mainly due to the smaller particle size, as well as higher inherent hardness of the B_4C particles. Furthermore, B_4C creates more geometrically necessary dislocations (GNDs) during thermal cycles due to the more pronounced different in thermal expansion coefficient [77]. Since B_4C particles are not deformed in the process, dislocations may be produced at their interfaces; therefore,

secondary slip must occur locally around each particle when the matrix is deformed. The density of secondary dislocations rises with increasing strain, and acts as a forest (dislocation forest) to impede the movement of the primary glide dislocations.

Figure 36 shows the relationship between microhardness and particle volume fraction for the different particles studied. This provides a direct comparison of the efficiency of reinforcement for multiple types of particles and sizes. The slope of hardness-volume fraction for the SiC and 130 nm Al_2O_3 reinforced composites is higher than 1.1 μm and 4.3 μm Al_2O_3 reinforced composites showing that with small increase in the volume fraction of SiC particle, the hardness increases sharply from 110 to 162 VHN.

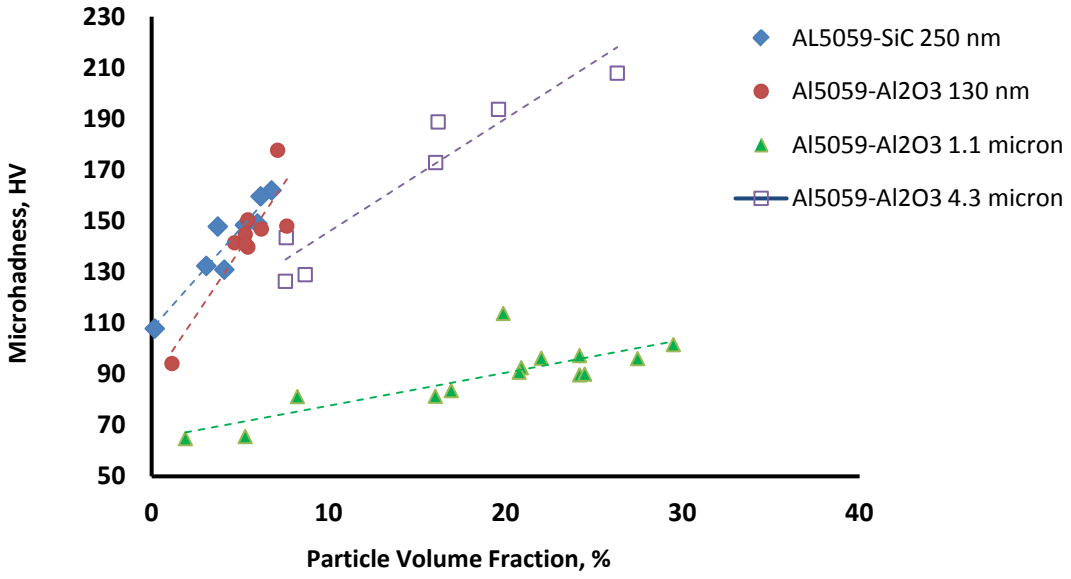

Figure 36: Average stir zone hardness value versus particle volume fraction for various composites produced by FSP.

It is considered that this due to the grain refinement (*i.e.* recrystallization process through FSP) and the high hardness of the SiC particles. That is, the FSP with the SiC particles is believed to make grains refinement process more effective due to the development of the induced strain and the pinning effect by the SiC particles (SiC possess an excellent pinning effect [28]). Likewise, it has been shown that the grain refinement in the FSP region is explained by the well-known Zener pinning effect, not only contributed by the presence of fine reinforcing particles, but also due to the break-up of dispersoid particles in the Al 5059 alloy itself, and this limits grain growth as the FSP region cools behind the trailing edge of the tool [82].

It has been reported that the stirring of material by the FSP tool has a substantial influence on the reinforcement particle size, morphology and distribution in the weld zone [78] as well as the evolution of grain structure of the matrix (*i.e.* alumnium). SEM micrographs (Figure 37) show that, 4.3 μm Al_2O_3 particles have been fragmented to smaller particles through FSP compared to the 1.1-μm Al_2O_3 particles. As evident in the micrographs, FSP has effectively broken the 1.1 and 4.3 μm sized particles down to smaller sizes.. The 4.3 μm Al_2O_3 particles are more severely broken by FSP than of 1.1 μm particles and refined to almost a 10 times smaller size following FSP, while FSP process refined the 1.1 μm particles to approximately half of their original size. Clearly, abrasion with the tool during FSP is responsible for some particle fracture; however there must be another mechanism to account for the more severe fragmentation of the 4.3 μm Al_2O_3 particles compared to the 1.1 μm ones. It is likely that the material flow around the tool within the stir zone promotes attrition of the particles with each other, and this is more efficient when there is a large population of larger particles available. As a result of the smaller inter- particle spacing, the numbers of collisions are way higher in the 4.3 μm particles than that of 1.1 μm leading to more refining in 4.3 μm particles. Image analyses of the SEM micrographs (Figure 38) suggest that there is a higher fraction of <0.5 μm particles in the 4.3 μm sized powder as compared with 1.1 μm sized particles. The 4.3 μm particle containing composite includes 72% of <0.5 μm particles, but the 1.1 μm consists of only 55% of <0.5 μm particles indicating the refinement has not been as effective.

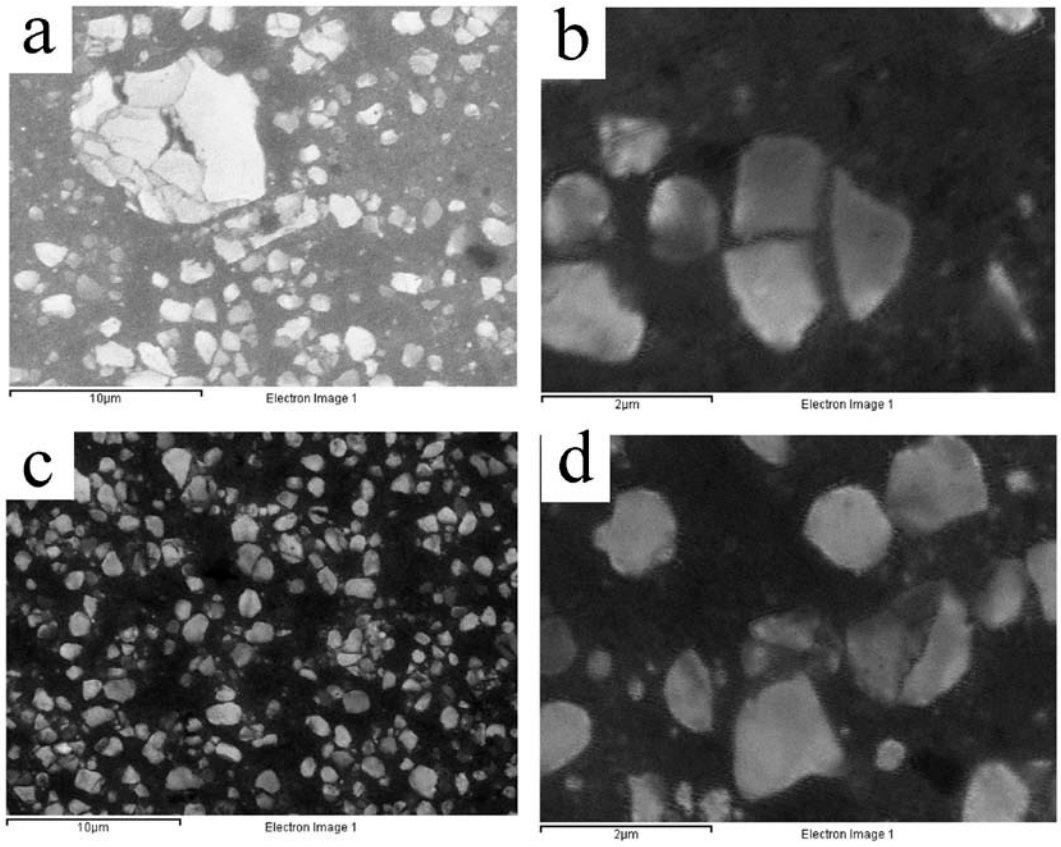

Figure 37: Scanning electron micrographs of friction stir processed samples containing a, b) 4.3 µm Al_2O_3 and c, d) 1.1µm Al_2O_3.

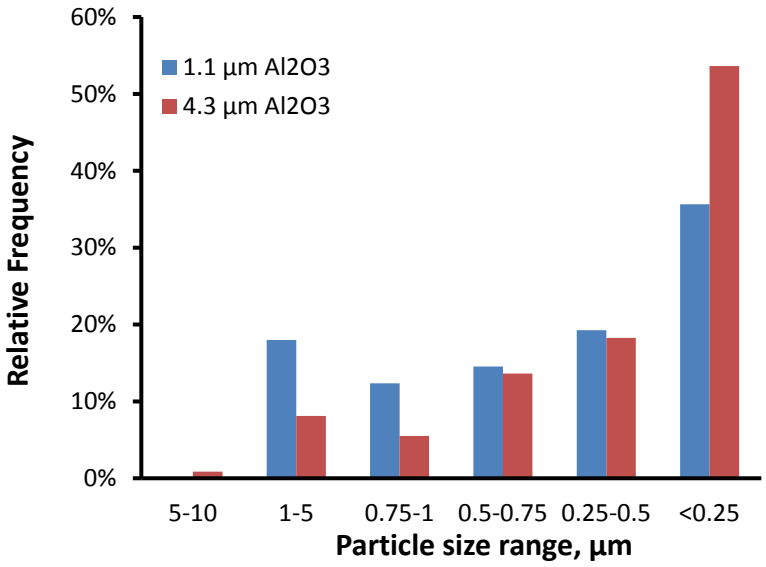

Figure 38: Size distribution of alumina particles in FSP composites produced using 1.1 µm vs. 4.3 µm Al_2O_3 particles.

Figure 39 compares the representative engineering flow curves of the fabricated composites. Figure 39 summarizes mechanical properties of the composites and base material. It can be noted that the reinforcement particles have a significant impact on the strength, particularly in the case of the B_4C reinforced material, which is consistent with the hardness values shown in Figure 35. However, the B_4C reinforced composite also exhibited brittle behaviour with the lowest ductility of all the studied composites (B_4C improve the strength at the expense of ductility).

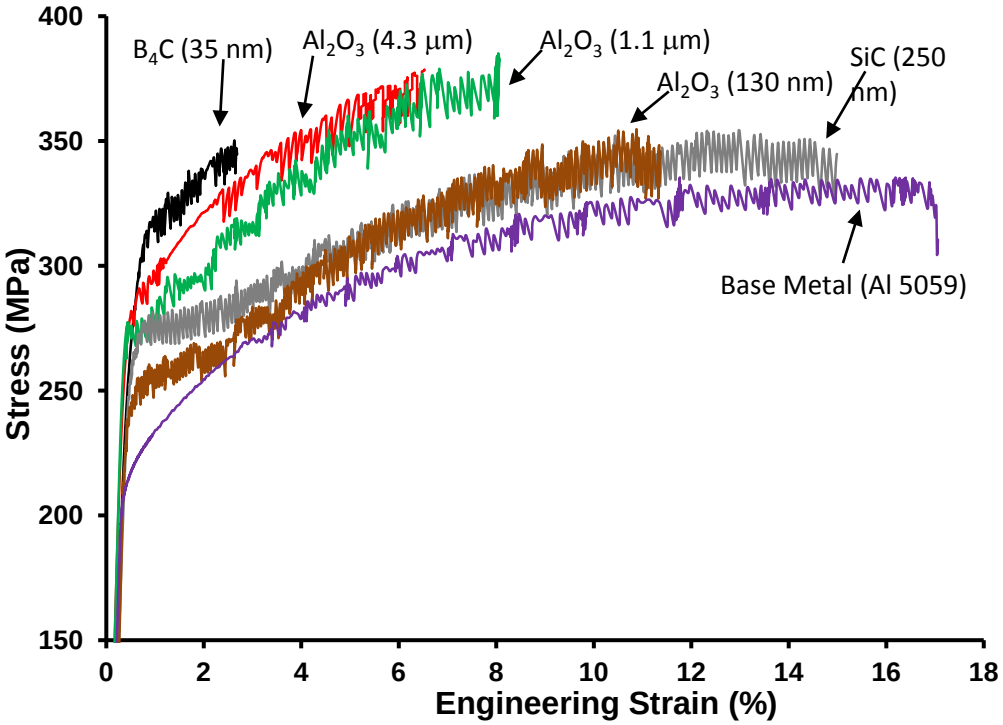

Figure 39: Tensile test results of FSP composites as compared with the base metal (Al 5059).

The improvement in strength properties of the fabricated composites can also be attributed to (*i*) effective load transfer from matrix to second phases due to the presence of fine reinforcements, (*ii*) considerable grain refinement due to enhanced matrix dynamic recrystallization and (*iii*) mismatch in elastic and thermal expansion coefficients between matrix and reinforcements (α_{B4C}= 5e-6, α_{SiC}= 4e-6, α_{Al2O3}= 8.4e-6, and α_{Al5059}= 24e-6 /°C) [79].

Table 6: Mechanical characteristics of base material and friction stir processed components

	YS (MPa)	UTS (MPa)	El (%)
Al5059	210	332	17
60 nm-Al_2O_3	233	353	11
60 nm-SiC	252	350	15
1.1 µm-Al_2O_3	272	368	8
4.3 µm-Al_2O_3	277	375	6.5
35 nm-B_4C	290	350	2.5

As is seen in Figure 40 pronounced strain hardening behavior is observed in the FSP Al-based composites as compared with base metal. If one ranks the materials from the highest to lowest hardening rate (y-axis), the B_4C is highest, yet it has the lowest strain. We would expect that the high strain hardening rate would suppress the fracture; however this may not have been accomplished for B_4C, since we also see the fracture surfaces are rather flat with little evidence of plastic deformation or strain accommodation just before fracture. The work hardening rate in Al_2O_3 130 nm and 1.1 μm are higher than the base metal which is in agreement with the results of Hu *et al.* [80]. These particles promote the pinning of active dislocations and grain boundaries of recrystallized grains. That is, uniformly distributed second particles in the friction stir processed samples can create, drag and hold (pin) dislocations causing dynamic recovery to be postponed.

The SiC is changing the hardening rate over the strains and the ranking is changing. It has been showed that the stress concentration around inclusions lead to embrittlement when a critical size was reached around 400 nm [81]. The 130 nm and 1.1 μm actually had final particle sizes both <300 nm it seems based on the SEM results, so it may be consistent with this stress concentration issue which promotes void nucleation. The Al_2O_3-4.3 μm shows a low work hardening rate because the large particles most likely promote void nucleation and de-cohesion before strain hardening can become active.

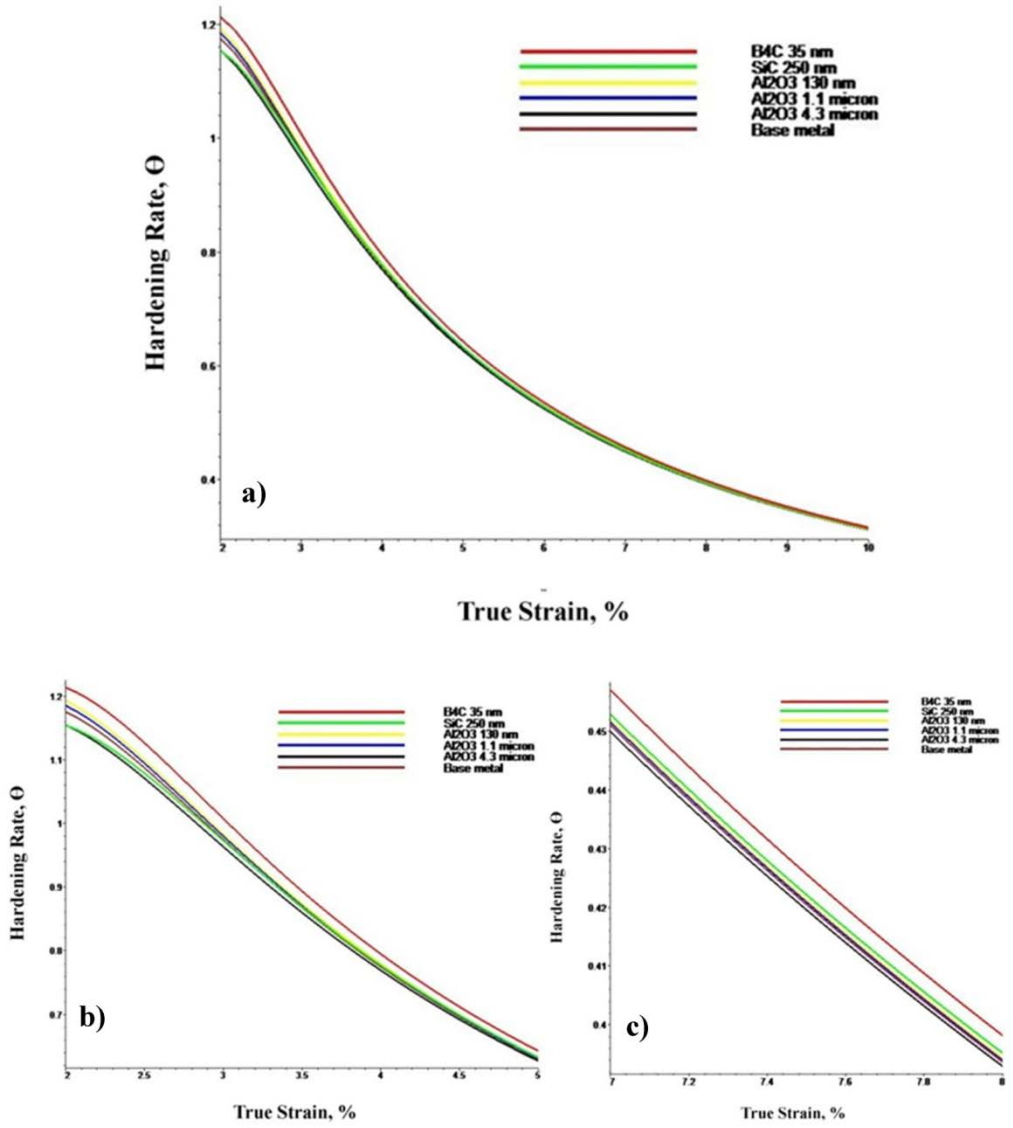

Figure 40: work hardening rate against the true plastic strain in friction stir proceed composites and base metal.

Figure 41 shows the fracture surfaces of Al_2O_3, SiC, and B_4C reinforced composites at different magnifications. Examination of the fractured surfaces at high magnification reveals equiaxed dimples on the fracture surface. The dimples are traces of micro voids produced during fracture which confirm ductile fracture behaviour in these composites. This is consistent with flow curves of Al_2O_3 and SiC reinforced composites shown in Figure 39 However, the fracture surface of B_4C reinforced composite

is nearly devoid of dimples or fibrous fracture surfaces, and this is consistent with the brittle behavior demonstrated in Figure 39.

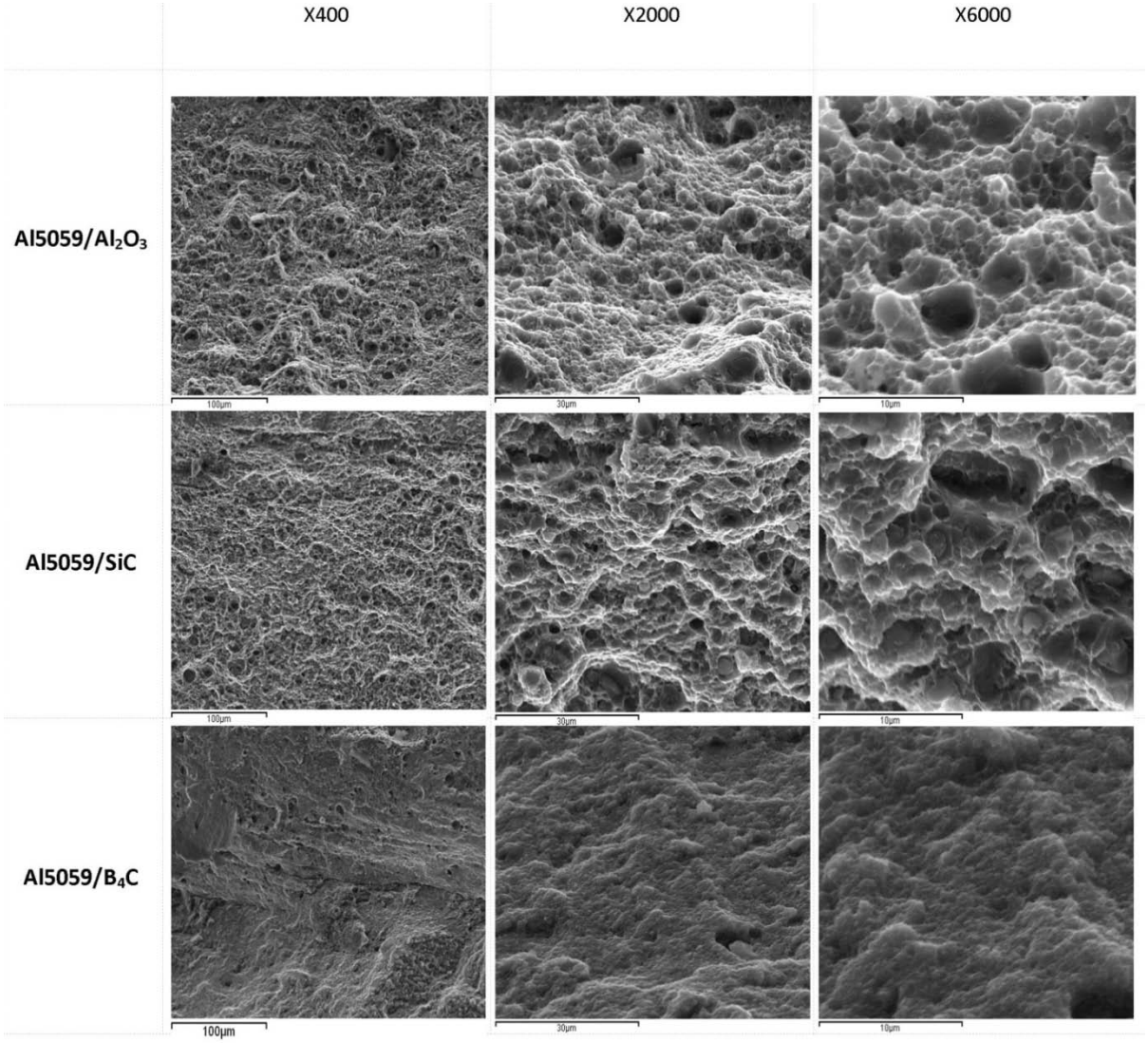

Figure 41: Fracture surface of Al2O3 (130 nm), SiC, and B4C reinforced composites.

Chapter 5
Conclusions

Metal matrix composites were successfully produced using friction stir processing by incorporating various reinforcement particles in different sizes. The influence of particle type and size distribution was studied in Al-alloy metal matrix composites produce by FSP. The mechanical and fracture behaviour was compared between the composites, and the main findings were that:

- By increasing the number of FSP passes, the distribution of reinforcing particles was much more homogeneous in the upper and lower portions of the stir zone.
- 3-pass friction stir processed composites made using a 2-mm groove and reinforced by particles shows an increase of ~15% in the hardness profile as compared with friction stir processed composite with no particles. This clearly confirms the effect of particles inclusion on the hardness profile.
- B_4C-reinforced composites exhibit the highest tensile yield strength; however their ductility is drastically reduced to 2.5% elongation in comparison to base metal.
- When using 4.3-μm Al_2O_3 particles, the FSP technique results in a 10 times refinement in the particle, while 1.1-μm Al_2O_3 particles are only refined to approximately half of their original size due to the less effective attrition within the severely deformed stir zone.
- The fracture surfaces confirm ductile fracture in the Al_2O_3-, SiC-reinforced composites and brittle fracture in the B_4C-reinforced composite, consistent with observed tensile flow curves.

Bibliography

[1] A. H. Feng and Z. Y. Ma, "Enhanced mechanical properties of Mg-Al-Zn cast alloy via friction stir processing," Scripta Materialia, vol. 56, pp. 397-400, 2007.

[2] W. M. Thomas, E. D. Nicholas, J. D. Needham, M. G. Murch, P. Templesmith, and C. J. Daws, 1991.

[3] R. S. Mishra and Z. Y. Ma, "Friction stir welding and processing," Materials Science and Engineering R: Reports, vol. 50, 2005.

[4] H. S. Arora, H. Singh, and B. K. Dhindaw, "Some observations on microstructural changes in a Mg-based AE42 alloy subjected to friction stir processing," Metallurgical and Materials Transactions B: Process Metallurgy and Materials Processing Science, vol. 43, pp. 92-108, 2012.

[5] P. Cavaliere and P. P. De Marco, "Friction stir processing of AM60B magnesium alloy sheets," Materials Science and Engineering A, vol. 462, pp. 393-397, 2007.

[6] C. B. Fuller and M. W. Mahoney, "The effect of friction stir processing on 5083-H321/5356 Al arc welds: Microstructural and mechanical analysis," Metallurgical and Materials Transactions A: Physical Metallurgy and Materials Science, vol. 37, pp. 3605-3615, 2006.

[7] M. D. Fuller, S. Swaminathan, A. P. Zhilyaev, and T. R. McNelley, "Microstructural transformations and mechanical properties of cast NiAl bronze: Effects of fusion welding and friction stir processing," Materials Science and Engineering A, vol. 463, pp. 128-137, 2007.

[8] K. Oh-Ishi and T. R. McNelley, "Microstructural modification of as-cast NiAl bronze by friction stir processing," Metallurgical and Materials Transactions A: Physical Metallurgy and Materials Science, vol. 35 A, pp. 2951-2961, 2004.

[9] M. Tsujikawa, S. W. Chung, M. Tanaka, Y. Takigawa, S. Oki, and K. Higashi, "High-strengthening of Mg - 5.5 mass % Y-4.3 mass % Zn cast alloy by friction stir processing," Materials Transactions, vol. 46, pp. 3081-3084, 2005.

[10] R. Bauri, D. Yadav, and G. Suhas, "Effect of friction stir processing (FSP) on microstructure and properties of Al-TiC in situ composite," Materials Science and Engineering A, vol. 528, pp. 4732-4739, 2011.

[11] P. B. Berbon, W. H. Bingel, R. S. Mishra, C. C. Bampton, and M. W. Mahoney, "Friction stir processing: A tool to homogenize nanocomposite aluminum alloys," Scripta Materialia, vol. 44, pp. 61-66, 2001.

[12] P. Cavaliere, "Mechanical properties of Friction Stir Processed 2618/Al2O3 metal matrix composite," Composites Part A: Applied Science and Manufacturing, vol. 36, pp. 1657-1665, 2005.

[13] K. J. Hodder, H. Izadi, A. G. McDonald, and A. P. Gerlich, "Fabrication of aluminum–alumina metal matrix composites via cold gas dynamic spraying at low pressure followed by friction stir processing," Materials Science and Engineering: A, vol. 556, pp. 114-121, 2012.

[14] Y. Morisada, H. Fujii, T. Mizuno, G. Abe, T. Nagaoka, and M. Fukusumi, "Modification of thermally sprayed cemented carbide layer by friction stir processing," Surface and Coatings Technology, vol. 204, pp. 2459-2464, 2010.

[15] Y. Morisada, H. Fujii, T. Nagaoka, and M. Fukusumi, "MWCNTs/AZ31 surface composites fabricated by friction stir processing," Materials Science and Engineering A, vol. 419, pp. 344-348, 2006.
[16] C. J. Lee, J. C. Huang, and P. J. Hsieh, "Mg based nano-composites fabricated by friction stir processing," Scripta Materialia, vol. 54, pp. 1415-1420, 2006.
[17] R. S. Mishra, Z. Y. Ma, and I. Charit, "Friction stir processing: A novel technique for fabrication of surface composite," Materials Science and Engineering A, vol. 341, pp. 307-310, 2003.
[18] P. Liu, Q. Shi, X. Bian, S. Xu, and G. Ren, "Microstructure of a novel Al-based amorphous reinforced aluminum metal matrix composite," Hanjie Xuebao/Transactions of the China Welding Institution, vol. 30, pp. 13-16, 2009.
[19] E. R. I. Mahmoud, M. Takahashi, T. Shibayanagi, and K. Ikeuchi, "Wear characteristics of surface-hybrid-MMCs layer fabricated on aluminum plate by friction stir processing," Wear, vol. 268, pp. 1111-1121, 2010.
[20] A. Tewari, J. E. Spowart, A. M. Gokhale, R. S. Mishra, and D. B. Miracle, "Characterization of the effects of friction stir processing on microstructural changes in DRA composites," Materials Science and Engineering A, vol. 428, pp. 80-90, 2006.
[21] W. Wang, Q. y. Shi, P. Liu, H. k. Li, and T. Li, "A novel way to produce bulk SiCp reinforced aluminum metal matrix composites by friction stir processing," Journal of Materials Processing Technology, vol. 209, pp. 2099-2103, 2009.
[22] A. Shafiei-Zarghani, S. F. Kashani-Bozorg, and A. Zarei-Hanzaki, "Microstructures and mechanical properties of Al/Al2O3 surface nano-composite layer produced by friction stir processing," Materials Science and Engineering A, vol. 500, pp. 84-91, 2009.
[23] M. Yang, C. Xu, C. Wu, K. C. Lin, Y. J. Chao, and L. An, "Fabrication of AA6061/Al2O3 nano ceramic particle reinforced composite coating by using friction stir processing," Journal of Materials Science, vol. 45, pp. 4431-4438, 2010.
[24] M. Dixit, J. W. Newkirk, and R. S. Mishra, "Properties of friction stir-processed Al 1100-NiTi composite," Scripta Materialia, vol. 56, pp. 541-544, 2007.
[25] D. K. Lim, T. Shibayanagi, and A. P. Gerlich, "Synthesis of multi-walled CNT reinforced aluminium alloy composite via friction stir processing," Materials Science and Engineering A, vol. 507, pp. 194-199, 2009.
[26] L. B. Johannes, L. L. Yowell, E. Sosa, S. Arepalli, and R. S. Mishra, "Survivability of single-walled carbon nanotubes during friction stir processing," Nanotechnology, vol. 17, pp. 3081-3084, 2006.
[27] H. Izadi and A. P. Gerlich, "Distribution and stability of carbon nanotubes during multi-pass friction stir processing of carbon nanotube/aluminum composites," Carbon, vol. 50, pp. 4744-4749, 2012.
[28] Y. Morisada, H. Fujii, T. Nagaoka, K. Nogi, and M. Fukusumi, "Fullerene/A5083 composites fabricated by material flow during friction stir processing," Composites Part A: Applied Science and Manufacturing, vol. 38, pp. 2097-2101, 2007.
[29] D. Yadav and R. Bauri, "Nickel particle embedded aluminium matrix composite with high ductility," Materials Letters, vol. 64, pp. 664-667, 2010.
[30] L. Zhang, R. Chandrasekar, J. Y. Howe, M. K. West, N. E. Hedin, W. J. Arbegast, et al., "A Metal Matrix Composite Prepared from Electrospun TiO2 Nanofibers and an Al 1100 Alloy via Friction Stir Processing," Applied Materials and Interfaces, vol. 1, pp. 987-991, 2009.
[31] C. I. Chang, Y. N. Wang, H. R. Pei, C. J. Lee, X. H. Du, and J. C. Huang, "Microstructure and Mechanical Properties of Nano-ZrO2 and Nano-SiO2 Particulate Reinforced AZ31-Mg

Based Composites Fabricated by Friction Stir Processing," Key Engineering Materials, vol. 351, pp. 114-119, 2007 2007.
[32] Y. Morisada, H. Fujii, T. Nagaoka, and M. Fukusumi, "Effect of friction stir processing with SiC particles on microstructure and hardness of AZ31," Materials Science and Engineering A, vol. 433, pp. 50-54, 2006.
[33] Y. Morisada, H. Fujii, T. Nagaoka, and M. Fukusumi, "Nanocrystallized magnesium alloy - uniform dispersion of C₆₀ molecules," Scripta Materialia, vol. 55, pp. 1067-1070, 2006.
[34] M. Barmouz, M. K. Besharati Givi, and J. Seyfi, "On the role of processing parameters in producing Cu/SiC metal matrix composites via friction stir processing: Investigating microstructure, microhardness, wear and tensile behavior," Materials Characterization, vol. 62, pp. 108-117, 2011.
[35] W. Chen, C. Huang, and L. Ke, "A novel way to fabricate carbon nanotubes reinforced copper matrix composites by Friction Stir Processing," vol. 391-392, ed. Shenyang, Liaoning, 2012, pp. 524-529.
[36] R. Salekrostam, M. K. B. Givi, P. Asadi, and P. Bahemmat, "Influence of friction stir processing parameters on the fabrication of SiC/316L surface composite " Deffects and Diffusion Forum, vol. 297-301, pp. 221-226, 2010.
[37] A. Ghasemi-Kahrizsangi and S. F. Kashani-Bozorg, "Microstructure and mechanical properties of steel/TiC nano-composite surface layer produced by friction stir processing," Surface and Coatings Technology, vol. 209, pp. 15-22, 2012.
[38] E. R. I. Mahmoud, M. Takahashi, T. Shibayanagi, and K. Ikeuchi, "Effect of friction stir processing tool probe on fabrication of SiC particle reinforced composite on aluminium surface," Science and Technology of Welding and Joining, vol. 14, pp. 413-425, 2009.
[39] L. Ke, C. Huang, L. Xing, and K. Huang, "Al-Ni intermetallic composites produced in situ by friction stir processing," Journal of Alloys and Compounds.
[40] C. J. Hsu, C. Y. Chang, P. W. Kao, N. J. Ho, and C. P. Chang, "Al-Al3Ti nanocomposites produced in situ by friction stir processing," Acta Materialia, vol. 54, pp. 5241-5249, 2006.
[41] C. J. Hsu, P. W. Kao, and N. J. Ho, "Intermetallic-reinforced aluminum matrix composites produced in situ by friction stir processing," Materials Letters, vol. 61, pp. 1315-1318, 2007.
[42] C. J. Hsu, P. W. Kao, and N. J. Ho, "Ultrafine-grained Al-Al2Cu composite produced in situ by friction stir processing," Scripta Materialia, vol. 53, pp. 341-345, 2005.
[43] E. R. I. Mahmoud, K. Ikeuchi, and M. Takahashi, "Fabrication of SiC particle reinforced composite on aluminium surface by friction stir processing," Science and Technology of Welding and Joining, vol. 13, pp. 607-618, 2008.
[44] M. Azizieh, A. H. Kokabi, and P. Abachi, "Effect of rotational speed and probe profile on microstructure and hardness of AZ31/Al 2O 3 nanocomposites fabricated by friction stir processing," Materials and Design, vol. 32, pp. 2034-2041, 2011.
[45] S. J. Vijay and N. Murugan, "Influence of tool pin profile on the metallurgical and mechanical properties of friction stir welded Al–10wt.% TiB2 metal matrix composite," Materials & Design, vol. 31, pp. 3585-3589, 2010.
[46] W. M. Thomas, E. D. Nicholas, and S. D. Smith, "Friction stir welding-tool developments," in Aluminum Automotive and Joining Sessions, Warrendale, PA, 2001.
[47] H. Izadi, "Effect of Friction Stir Processing Parameters on Microstructure and Mechanical Properties of AL 5059," in 9th International Conference on Trends in Welding Research, 2012.
[48] W. D. Callister, Materials Science and Engineering, An Introduction. York, PA: John Wiley & Sons, Inc., 2007.

[49] R. H. Krock, in ASTM Proceeding Philadelphia, PA, 1963.
[50] K. U. Kainer, Metal Matrix Composites. Custom-made Materials for Automotive and Aerospace Engineering. Weinheim: WILEY-VCH Verlag GmbH & Co. KGaA, , 2006.
[51] M. Rosso, "Ceramic and metal matrix composites: Routes and properties," Materials Processing Technology, vol. 175, pp. 364–375, 2006.
[52] F. Cardarelli, Materials Handbook A Concise Desktop Reference. London: Springer-Verlag London Limited, 2008.
[53] T. W. Clyne and P. J. Withers, An Introduction to Metal Matrix Composites. Cambridge: Cambridge University Press, 1993.
[54] C. R. Kennedy, "Proceedings of the 7th CIMTEC-World Ceramics Congress," in Elsevier, New york, 1991, p. 691.
[55] C. K. Kumar, Composite materials: science and engineering. New York: Springer, 2012.
[56] A. J. Cook and P. S. Werner, "Pressure infiltration casting of metal matrix composites," Materials Science and Engineering: A, vol. 144, pp. 189-206, 1991.
[57] R. Saha, E. Morris, N. Chawla, and S. M. Pickard, "Hybrid and Conventional Particle Reinforced Metal Matrix Composites by Squeeze Infiltration Casting," Mater. Sci. Lett, vol. 21, pp. 337-339, 2002.
[58] S. Nourbakhsh, F. L. Liang, and H. Margolin, "Interaction of Al2O3-ZrO2 fibres with a Ti-Al matrix during pressure casting," Metallurgical Transactions A, vol. 21A, pp. 213–219, 1990.
[59] K. k. Chawla and L. B. Godfroid, "Faracture behavior of Al 1100/Al 2024 laminate Composites " in Proceedings of the 6th International Conference on Fracture (ICF6), New Delhi, India, 1984.
[60] W. H. Hunt, "Processing and Fabrication of Advanced Materials," in The Minerals and Metal Materials Society, Warrendale, Pa, 1994, p. 663−683.
[61] N. Chawla, J. J. Williams, and R. Saha, J. Light Metals, vol. 2, pp. 215-227, 2002.
[62] J. C. Halpin and S. W. Tsai, "Air Force Materials Laboratory," AFML-TR, pp. 67-423, 1967.
[63] Z. Y. Ma, R. S. Mishra, and M. W. Mahoney, "Superplastic deformation behaviour of friction stir processed 7075Al alloy," Acta Materialia, vol. 50, pp. 4419-4430, 2002.
[64] R. S. Mishra, M. W. Mahoney, S. X. McFadden, N. A. Mara, and A. K. Mukherjee, "High strain rate superplasticity in a friction stir processed 7075 Al alloy," Scripta Materialia, vol. 42, pp. 163-168, 2000.
[65] R. S. Mishra, Z. Y. Ma, and I. Charit, "Friction stir processing: a novel technique for fabrication of surface composite," Materials Science and Engineering: A, vol. 341, pp. 307-310, 2003.
[66] Z. Y. Ma, "Friction Stir Processing Technology: A Review," Metallurgical And Materials Transactions A, vol. 39 A, pp. 642-658, 2008.
[67] R. S. Mishra and Z. Y. Ma, "Friction stir welding and processing," Materials Science and Engineering, vol. 50, pp. 1-78, 2005.
[68] I. Charit and R. S. Mishra, "High strain rate superplasticity in a commercial 2024 Al alloy via friction stir processing," Materials Science and Engineering: A, vol. 359, pp. 290-296, 2003.
[69] P. Su, A. Gerlich, T. H. North, and G. J. Bendzsak, "Intermixing in dissimilar friction stir spot welds," Metallurgical and Materials Transactions A: Physical Metallurgy and Materials Science, vol. 38, pp. 584-595, 2007.
[70] P. Asadi, M. K. Besharati Givi, K. Abrinia, M. Taherishargh, and R. Salekrostam, "Effects of SiC Particle Size and Process Parameters on the Microstructure and Hardness of AZ91/SiC Composite Layer Fabricated by FSP," Materials Engineering and Performance, vol. 20, pp. 1554-1562, 2011.

[71] P. Cavaliere, "Mechanical properties of Friction Stir Processed 2618/Al2O3/20p metal matrix composite," Composites Part A: Applied Science and Manufacturing, vol. 36, pp. 1657–1665, 2005.
[72] Y. H. Yin, N. Sun, T. H. North, and S. S. Hu, "Influence of tool design on mechanical properties of AZ31 friction stir spot welds," Science and Technology of Welding and Joining, vol. 15, pp. 81-86, 2010.
[73] N. Sun and D. Apelian, "Friction Stir Processing of Aluminum Cast Alloys for. High Performance Applications," JOM, vol. 63, pp. 44-50, 2011.
[74] R. Nandan, G. G. Roy, and T. Debroy, "Numerical simulation of three dimensional heat transfer and plastic flow during friction stir welding," Metallurgical and Materials Transactions A: Physical Metallurgy and Materials Science, vol. 37, pp. 1247-1259, 2006.
[75] Y. Morisada, H. Fujii, T. Nagaoka, and M. Fukusumi, "Effect of friction stir processing with SiC particles on microstructure and hardness of AZ31," Material Science and Engineering A, vol. 433, pp. 50-54, 2006.
[76] A. Gerlich, M. Yamamoto, and T. H. North, "Strain rates and grain growth in Al 5754 and Al 6061 friction stir spot welds," Metallurgical and Materials Transactions A: Physical Metallurgy and Materials Science, vol. 38, pp. 1291-1302, 2007.
[77] H. Izadi, A. Nolting, C. Munro, D. P. Bishop, K. P. Plucknett, and A. Gerlich, "Friction stir processing of Al/SiC composites fabricated by powder metallurgy," Materials Processing and Technology, vol. 213, pp. 1900-1907, 2013.
[78] X.-G. Chen, "Microstructure and mechanical properties of friction stir welded AA6063–B4C metal matrix composites," Materials Science and Engineering A, pp. 174-184, 2009.
[79] S. Sankaranarayanan, S. Jayalakshmi, and M. Gupta, "Hybridizing micro-Ti with nano-B4C particulates to improve the microstructural and mechanical characteristics of Mg–Ti composite," Journal of Magnesium and Alloys, vol. 2, pp. 13-19, 2014.
[80] C. M. Hu, C. M. Lai, X. H. Du, N. J. Ho, and C. Huang, "Enhanced tensile plasticity in ultrafine-grained metallic composite fabricated by friction stir process," Scripta Materialia, vol. 59, pp. 1163-1166, 2008.
[81] W. W. B. F. A. L. M. C. P. Bowen, "Micromechanisms of cleavage fracture initiation from inclusions in ferritic welds: Part II. Quantification of local fracture behaviour observed in fatigue pre-cracked testpieces," Materials Science and Engineering: A, vol. 452-453, pp. 401-410, 2007.
[82] H. Izadi, R. Sandstrom, and A. P. Gerlich, "Grain Growth Behavior and Hall–Petch Strengthening in Friction Stir Processed Al 5059," Metallurgical and Materials Transactions A, pp. 1-10, 2014.